minerals

MDPI

Article

Linking Gold Systems to the Crust-Mantle Evolution of Archean Crust in Central Brazil

Jessica Bogossian *, Anthony I. S. Kemp and Steffen G. Hagemann

Centre for Exploration Targeting, School of Earth Sciences, University of Western Australia, Perth 6009, Australia; tony.kemp@uwa.edu.au (A.I.S.K.); steffen.hagemann@uwa.edu.au (S.G.H.)
* Correspondence: jessicabogossian@gmail.com

Abstract: The Goiás Archean Block (GAB) in central Brazil is an important gold district that hosts several world-class orogenic gold deposits. A better comprehension of the crustal, tectono-magmatic, and metallogenic settings of the GAB is essential to accurately define its geological evolution, evaluate Archean crustal growth models, and target gold deposits. We present an overview of gold systems, regional whole-rock Sm-Nd analyses that have been used to constrain the geological evolution of the GAB, and augment this with new in situ zircon U-Pb and Hf-O isotope data. The orogenic gold deposits show variable host rocks, structural settings, hydrothermal alteration, and ore mineralogy, but they represent epigenetic deposits formed during the same regional hydrothermal event. The overprinting of metamorphic assemblages by ore mineralogy suggests the hydrothermal event is post-peak metamorphism. The metamorphic grade of the host rocks is predominantly greenschist, locally reaching amphibolite facies. Isotope-time trends support a Mesoarchean origin of the GAB, with ocean opening at 3000–2900 Ma, and reworking at 2800–2700 Ma. Crustal growth was dominated by subduction processes via in situ magmatic additions along lithospheric discontinuities and craton margins. This promoted a crustal architecture composed of young, juvenile intra-cratonic terranes and old, long-lived reworked crustal margins. This framework provided pathways for magmatism and fluids that drove the gold endowment of the GAB.

Keywords: gold systems; crustal evolution; Goiás Archean Block; central Brazil

check for updates

Citation: Bogossian, J.; Kemp, A.I.S.; Hagemann, S.G. Linking Gold Systems to the Crust-Mantle Evolution of Archean Crust in Central Brazil. *Minerals* **2021**, *11*, 944. https://doi.org/10.3390/min11090944

Academic Editor: Silvio Giuseppe Rotolo

Received: 2 June 2021
Accepted: 26 August 2021
Published: 30 August 2021

1. Introduction

The formation of orogenic gold deposits in the Neoarchean, Paleoproterozoic, and Phanerozoic is associated with accretionary to collisional tectonics along convergent lithospheric boundaries that precede the stabilization of the subcontinental lithospheric mantle [1,2]. The major controls on the development of large orogenic gold deposits include age, temperature, and lithospheric thickness [2,3]. Enhanced asthenospheric heat input, typical of an unstable or delaminated subcontinental lithospheric mantle, promotes the devolatilization of sedimentary and/or volcanic rocks that produce metamorphic fluids in well-endowed gold provinces [4,5]. Consequently, a better understanding of the crust-mantle interactions through time and lithospheric architecture has a direct impact on the economic exploration of mineral systems [6–8].

The Goiás Archean Block (GAB), the only Archean terrane recognized in central Brazil (Figure 1A), was amalgamated into the Neoproterozoic Tocantins Province during the Brasiliano/Pan-African orogeny [9]. It consists of typical granite-gneiss TTG complexes and associated greenstone belts (Figure 1B). Despite its relatively small size (ca. 50,000 km^2), the GAB hosts several economically important gold deposits. These include the world-class Serra Grande mine, in the Crixás greenstone belt (≤7 Moz Au; AngloGold Ashanti), and deposits hosted in the Pilar de Goiás and Guarinos greenstone belts (6.5 Moz, Yamana Gold Inc.). Gold systems are hosted predominantly in Archean-Paleoproterozoic greenstone belts, and rarely in Neoproterozoic intrusions [10,11]. The deposits reveal a variety of mineralization styles, host rocks and structural settings [11,12], but they all show

strong structural control, CO_2, K, Fe, S enrichment, similar fluid conditions and hydrothermal alteration characteristics typical of orogenic deposits [1,13]. Field relationships and geochronology suggest these deposits formed during a regional hydrothermal event related to a Paleoproterozoic orogeny at ca. 2100 Ma [14–16].

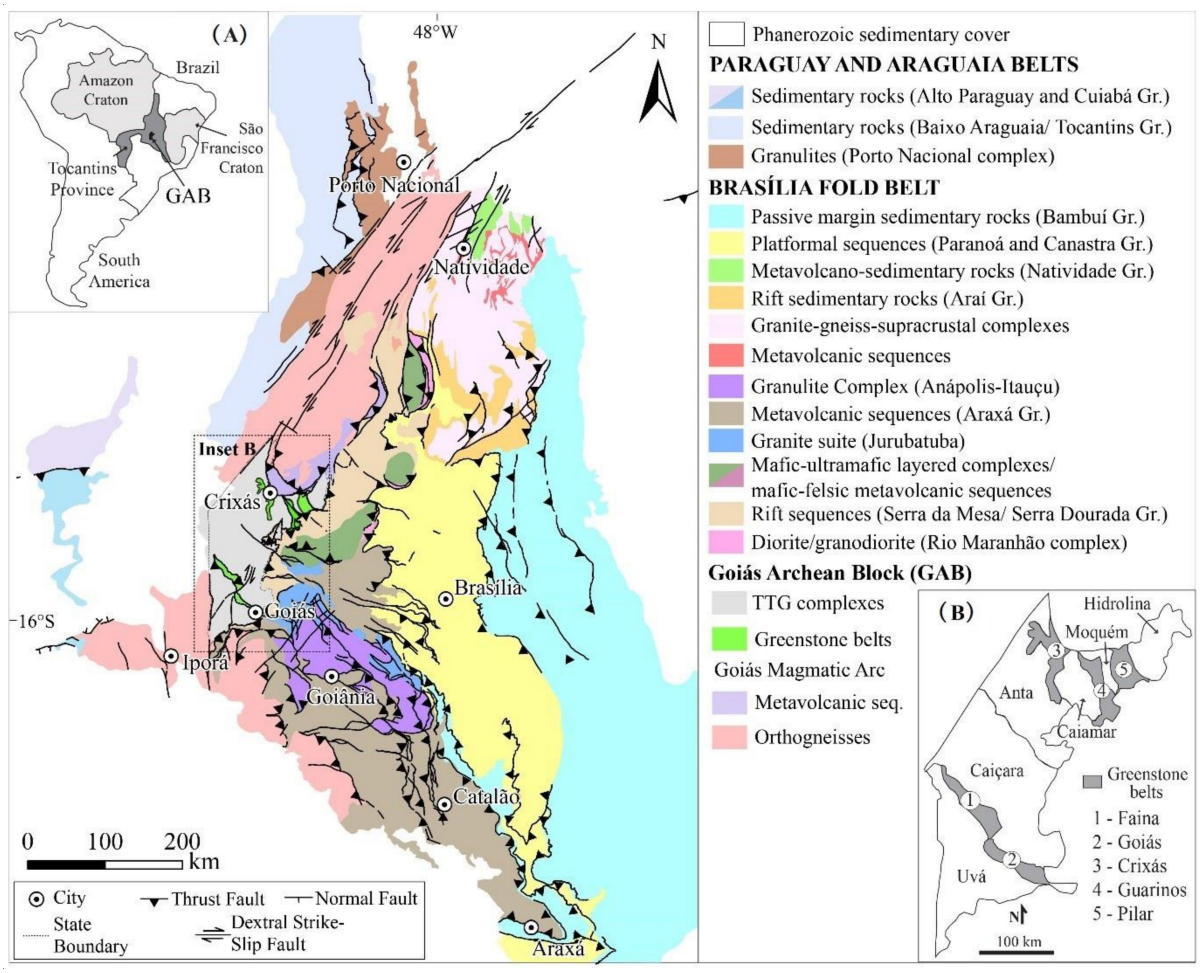

Figure 1. Geology of the Brasília fold belt (modified after Pimentel et al. [17]). (**A**): location of the GAB in South America; (**B**): greenstone belts and TTG terranes of the Goiás Archean Block.

Previous studies in the GAB have focused on the greenstone belts, as they are the most important host for gold deposits in the region [11,18–20]. Available data throughout the GAB is highly variable, with most studies focused on the north [21–23], and comparatively little work carried out in the south [24–26]. This can be partially explained by the long history of mining activity in the northern greenstone belts. Limited work in the TTG complexes, including U-Pb geochronology, Sm-Nd isotopic studies, and whole-rock geochemistry have shown that the crustal architecture of the GAB is composed of discrete lithospheric blocks of varying age, composition, and origin [21–28]. However, none of these studies have linked the isotopic characteristics of these blocks to the localization of mineral systems, as proposed for other cratonic areas such as the Yilgarn Craton, in Western Australia [29]. The ambiguous nature and still unclear origin of the GAB makes the area an exciting case study to investigate relations between crustal evolution and distribution of mineral systems.

The purpose of this work is to provide an updated appraisal of existing literature including some newly acquired data on the regional geology of the main gold deposits followed by a model for the tectono-magmatic evolution of the GAB. This dataset is used to present a more robust understanding of the crustal evolution of the craton.

Results of whole-rock analyses, in situ zircon SHRIMP U-Pb geochronology and Hf-O isotopic analyses for eight intrusive rocks in the southern GAB are reported here (Sections 2 and 3). These results challenge the paradigm of the exotic nature of the craton. Isotopic consonance across terranes suggests crustal growth by successive magmatic additions from similar sources. This is consistent with a linked, rather than exotic, evolution of terranes. The second part of the paper presents a synthesis of geological characteristics of orogenic gold mineralization in the GAB based on existing literature including new data initially presented. The third part focuses on available chemical, geochronological and isotopic data used to provide a framework of the crust-mantle evolution for the area. Long-term controversy concerning Archean crustal growth is assessed to reconcile available models. The spatial framework obtained from this geological dataset is used to infer links between crustal evolution and mineral systems, particularly gold, in the GAB.

2. Material and Methods

New whole-rock geochemistry, zircon U-Pb geochronology and Hf-O isotope data were obtained from eight igneous rocks in the southern GAB. Whole-rock analyses were conducted by Bureau Veritas (Perth, Australia). The samples were cast using a 66:34 flux with 4% Lithium nitrate added to form a glass bead. Major element oxides were analysed by XRF (X-ray fluorescence spectrometry). The analyses of 51 trace elements utilized fused bead laser ablation (ICP-MS). Gold, Pt and Pd were measured by Inductively Coupled Plasma (ICP) Optical Emission Spectrometry. Carbon and S were quantified by total combustion analysis, and FeO was determined volumetrically after acid digestion. The Geological Survey of Western Australia (GSWA) rock standard KG1 (Kerba Monzogranite [30]) was analysed to monitor data quality. The geochemical analyses are available in the Supplementary Table S1.

Approximately 2 kg of each sample was crushed, milled, sieved (50 mesh), panned, and magnetically separated (Frantz) to obtain heavy mineral concentrates. Non-magnetic heavy minerals were separated using LST (lithium heteropolytungstates; density of 2.95 g/mL at 25 °C). The zircon grains were handpicked, mounted in epoxy discs, and polished into two mounts (JB 1 and JB 2). Each mount included reference zircons for quality control purposes. The zircon standards used for U-Pb dating were BR266 ($^{206}Pb/^{238}U$ and $^{207}Pb/^{206}Pb$ ages of 559.0 ± 0.5 Ma, 903 ppm U [31]) and OGC ($^{207}Pb/^{206}Pb$ age of 3465.4 0 ± 0.6 Ma, 903 ppm U [32]). All zircon grains were imaged using the Vega 3 Tescan Scanning Electron Microprobe (SEM-EDS) at the Centre for Microscopy, Characterisation and Analysis (CMCA) at UWA. Electronic microscopy included secondary electron (SE), backscatter (BSE), and cathodoluminescence (CL) images to study the morphology of the zircon grains, e.g., growth patterns, inclusions, and fractures, for spot location. The images were obtained using an accelerating voltage of 20 kV, a working distance of 15 mm, and a beam intensity of 1.5 nA.

Analysis of selected zircons was conducted using the SHRIMP II (Sensitive High-mass Resolution Ion Microprobe) at the John de Laeter Centre (Curtin University), based on the methodology of Compston et al. [33]. Raw data was reduced with the program SQUID [34] and processed with IsoPlot v. 3.71 [35]. The U-Pb concordia diagrams, weighted average, and probability plots were plotted at a 95% confidence level (2σ).

Oxygen and hafnium isotope analyses were conducted in the same area of previous U-Pb dating. In situ Hf-O isotopic measurements were preferentially undertaken on zircon grains with less than 10% U-Pb age discordance. However, since ancient lead loss can also result in trends sub-parallel to the concordia over millions of years (e.g., [36]), concordance alone might be an unreliable disturbance index in Archean zircons [37]. Zircon oxygen isotope composition was measured by secondary ion mass spectrometry (SIMS) using a Cameca IMS 1280 multi-collector ion microprobe at the CMCA (UWA). Hafnium isotope analysis was conducted using a Thermo Scientific Neptune Plus multi-collector ICP-MS combined with a 193 nm Ar-F excimer laser sampling system in the School of Earth Sciences at UWA. The technique for oxygen analyses followed Nemchin et al. [38] and

Whitehouse and Nemchin [39], whereas analytical protocols for hafnium analyses followed Kemp et al. [40]. The data reproducibility was evaluated by quality control analysis using reference zircons Penglai, OGC, FC1, and Mud Tank. The εHf values for analysed sample zircons were calculated using a ^{176}Lu decay constant of 1.865×10^{-11} yr^{-1} [41], and the chondritic values of Bouvier et al. [42]. Averages of the U-Pb, Hf, and O isotope results for each sample are listed in Supplementary Table S2.

3. Results

3.1. Petrology

The investigated rocks of the southern GAB (Supplementary Figure S1) show varying degrees of deformation, represented by homogeneous to augen-like textures (Supplementary Figures S2 and S3). A summary of their mineralogy is presented below in Table 1.

Table 1. Summary of the mineralogy of the studies samples.

Sample	Lithology	Texture	Structure	Mineralogy	Description
Pink Syenite	Qtz Syenite	Porphyroclastic	Massive	KF-Plg ± Ms ± Qtz	Porphyritic K-feldspar (≤1 cm) in fin-grained (~50 µm) plagioclase-quartz matrix
Serra Negra	Monzonite	Phaneritic	Subtle foliation	Qtz-KF-Plg-Bt-Tit-Ep	Fine- to medium-grained granitic rock
Rio Caiapó	Monzonite	Phaneritic	Massive	Qtz-Plg-Bt-Ep-Aln	Medium-grained granite with mafic enclaves
Itapuranga I	Monzonite	Augen, porphyritic	Foliated	Qtz-KF-Plg-Hbl-Bt-Aln ± Ep	Medium- to coarse-grained granitic rock
Itapuranga II	Monzonite	Nematoblastic	Subtle foliation	Qtz-KF-Plg-Bt- ± Ep ± Aln	
Uvá	Orthogneiss	Augen gneiss	Intense foliation	Qtz-KF-Plg-Bt ± Ep ± Ap	Medium- to coarse-grained leucocratic orthogneiss composed of xenomorphic biotite and rare hornblende.
Caiçara	Orthogneiss	Phaneritic	Subtle foliation	Qtz-Plg-KF ± Ms ± Tit	
Paus de Choro	Two-mica granite	Nematoblastic	Subtle foliation	Qtz-KF-Plg-Bt ± Ms	

Abbreviations: Qtz: quartz, Plg: plagioclase, KF: K-feldspar, Ms: muscovite, Bt: biotite, Aln: allanite, Tit: titanite, Ep: epidote, Hbl: hornblende.

The SiO_2 content of the analysed samples ranges from 64.4 to 76.0 wt. % and the samples fall in the granite and quartz monzonite fields on the total alkalis-silica diagram of Middlemost [43]. K_2O/Na_2O ratios increase with decreasing age, except for the Serra Negra granite that shows values comparable to the ones of Archean intrusions.

In primitive mantle normalized diagrams [44,45], all samples show strong negative anomalies of high strength elements (HFSE), e.g., Ta, Nb, and Ti. Conversely, large ion lithophile elements (LILE) such as Cs, Ba, and Rb are enriched in Neoproterozoic intrusions when compared to the Archean/Paleoproterozoic intrusions. Pink Syenite and Rio Caiapó granite display a negative Eu anomaly, whereas Serra Negra and Itapuranga granites show anomalous high Ba and Sr contents.

3.2. SHRIMP Zircon U-Pb Geochronology

Geochronological results show three major peaks of igneous activity in the southern GAB during the Archean, Paleoproterozoic, and Neoproterozoic. Older magmatism is related to the formation of Archean TTGs between 2890–2820 Ma. Paleoproterozoic magmatism is represented by the 2060 Ma syn-orogenic Pink Syenite. In the Neoproterozoic two main age groups are defined by 630–610 Ma K-rich granites (i.e., Rio Caiapó, Itapuranga I and Itapuranga II) and 530 Ma Serra Negra granite. Results of SHRIMP U-Pb zircon geochronology are presented in Supplementary Tables S3 and S4. Cathodoluminescence images of representative zircon grains and concordia diagrams are provided in Supplementary Figures S4 and S5, respectively. Analyses of standard materials used for U-Pb geochronology are available in Supplementary Table S5.

3.3. In Situ Zircon Hf-O Analyses

Results of in situ Lu-Hf isotope geochemistry of investigated rocks in the southern GAB and standard materials used for quality control are available in Supplementary Tables S6 and S7, respectively. A plot of εHf versus crystallization and inheritance age of magmatic zircons from the southern GAB is provided in Supplementary Figure S6 [46–56]. Hafnium isotope composition of zircons of granitic rocks in the southern GAB entail four major groups: (i) near-chondritic εHf(t) values (+2.4 to −0.7) of Archean TTG intrusions (Caiçara, Uvá, and Paus de Choro), (ii) unradiogenic εHf(t) values (−8.3 to −10.6) of Paleoproterozoic Pink Syenite, (iii) unradiogenic εHf(t) values (−3.0 to −10.5) of Neoproterozoic K-rich granites (i.e., Rio Caiapó, Itapuranga I and II), and (iv) extremely unradiogenic εHf(t) values (−18.6 to −20.6) of Neoproterozoic Serra Negra granite. The extremely unradiogenic εHf(t) values registered for the latter plot on the extension of a trend delineated by the first group.

Results of in situ oxygen isotope measurements of investigated rocks in the southern GAB and standard materials used to calibrate oxygen analyses are available as Supplementary Tables S8 and S9, respectively. The zircon oxygen compositions are mostly heterogeneous within samples > 2060 Ma, with standard deviations comparable to that of the reference materials (0.2‰ < 2σ < 0.5‰; Supplementary Table S9). A plot of $\delta^{18}O$ versus emplacement age of granitic rocks in the southern GAB is provided in Supplementary Figure S7. Oxygen isotopic compositions between 2890–2820 Ma form a scattered range from 2.1% to 7.2‰, with higher values related to younger intrusions (i.e., Paus de Choro granite). A transition to heavier oxygen isotopic compositions is recorded by 2060 Ma Pink Syenite (5.8%–7.2‰). Following considerable shift to high-$\delta^{18}O$ zircons of 630–612 Ma K-rich granites (8.4%–10.7‰), $\delta^{18}O$ values rapidly decrease for the 530 Ma Serra Negra granite (5.6%–6.0‰).

4. Geological Setting

The collision of the Amazonian, São Francisco and Paranapanema cratons in the Brasiliano/Pan-African orogeny led to the formation of the Tocantins Province [57–59]. The province comprises the Brasília fold belt in the east and the Araguaia and Paraguay fold belts in the northeast and west, respectively [9]. The Brasília fold belt (BFB) is one of the most complete Neoproterozoic orogens of Western Gondwana [60]. It is subdivided into NNE–SSW trending and NNW–SSE trending branches, which are separated by the WNW–ESE trending Pirineus syntaxis [9,17,61]. Several tectonic domains are distinguished in the BFB [9,17,62–65]. Its eastern part consists of thick passive margin sedimentary sequences deformed under low greenschist facies metamorphism (Figure 1). In the northeast, the BFB is made up of a Paleoproterozoic granite-gneiss terrane containing minor volcano-sedimentary sequences known as the Natividade greenstone belt [66,67], and Meso- to Neoproterozoic layered mafic-ultramafic complexes [68]. Its western part is composed of: (i) a Neoproterozoic Anápolis-Itauçu granulite metamorphic core [69] and metasedimentary rocks of the Araxá Group [60]; (ii) Archean granite-greenstone terrains of the GAB [11]; (iii) a Neoproterozoic Goiás Magmatic Arc with calc-alkaline orthogneisses and volcano-sedimentary sequences [59,70], as well as several syn- to post-orogenic granite intrusions [26,27].

Several names have been attributed to the area encompassing the GAB, e.g., 'Goiás Archean Nuclei' [71], 'Crixás granite-greenstone belt terrane' [72], 'Archean terranes of Crixás-Goiás' [9], 'Goiás-Crixás Archean Block' [28], 'Goiás-Crixás Block' [73], 'Archean terrain of central Brazil' [74], 'Goiás Archean Block' [60,75,76], and 'Archean-Paleoproterozoic terrane of central Brazil' [11,77]. The term Goiás Archean Block (GAB) is adopted herein as a reference to the only example of exposed Archean crust in the Tocantins Province [28,57,62] and in the Goiás State.

The GAB, formed by approximately 70% granite-gneiss TTG association and 30% greenstone belts, records a chronological range from Archean to Paleoproterozoic rocks [75], with rare Neoproterozoic intrusions [10,28] (Figure 2).

The polycyclic evolution of the GAB, inferred from studies concerning Archean TTG magmatism, led to its subdivision into northern and southern portions [19,21,22]. The northern portion consists of two major magmatic stages: (i) juvenile, polydeformed batholith-like tonalite, granodiorite, and granite orthogneisses with SHRIMP U-Pb zircon ages between 2840–2780 Ma and εNd +2.4 to −1.0 (Caiamar and Anta terranes), and (ii) crustal-derived, dike-like granodiorite to granite gneisses with SHRIMP U-Pb zircon ages between ca. 2790–2700 Ma, and negative εNd of −2.2 (Moquém and Hidrolina terranes) [22]. The southern portion comprises the Uvá and Caiçara TTG terranes, separated by the Faina and Goiás greenstone belts (Figure 1B). Regional studies indicate the stabilization of the GAB at ca. 2700 Ma, with crustal extension between 2500–2300 Ma [78], and closure of accretionary orogens between 2300–2050 Ma [11,15]. The TTG terranes of the GAB consist of intensely deformed orthogneisses of variable composition and age that were first delineated by gamma-spectrometry [79]. Compositionally, TTG orthogneisses vary from tonalite to granodiorite, with minor granite, charnockite, monzogranite, and adakite-like [12,23]. Available geochronology shows that TTG terranes formed during several discrete episodes dating back to 3140 Ma [23], with most preserved intrusions emplaced at 2960–2840 Ma, 2845–2785 Ma, and 2790–2700 Ma [21,22,24,25,28,77]. The 2845–2785 Ma and 2960–2840 Ma episodes are the most widespread in the northern and southern GAB, respectively, and were broadly synchronous with Archean volcanism [21,22]. The 2790–2700 Ma episode is more common in the north, and it appears to be the last magmatic event in the GAB.

There are five greenstone belts in the GAB (Figure 3). In the north, three NNW-trending, subparallel inliers (ca. 40 km length and 6 km width) comprise, from west to east, the Crixás, Guarinos, and Pilar de Goiás greenstone belts. These greenstone belts were defined by Danni and Ribeiro [80], and Sabóia [81], with further description by Jost and Oliveira [18]. In the south, two NW-trending belts (ca. 60 km length and 5 km width) are represented, from west to east, by the Faina and Goiás greenstone belts. They both form a synclinorium offset by the NE-trending, dextral Faina fault [11,82]. The preservation of primary structures, e.g., upward younging in pelites, indicates that the southwestern limb of the Faina synclinorium is inverted whereas the northeastern limb is upright [82]. Based on the distribution of sedimentary sequences in the Faina and Goiás greenstone belts, their apparent right-lateral displacement, coupled with the contrasting sedimentation recorded in both sequences, the Faina Fault is inferred to represent a syn-sedimentary growth fault or a rift-related transform fault [82].

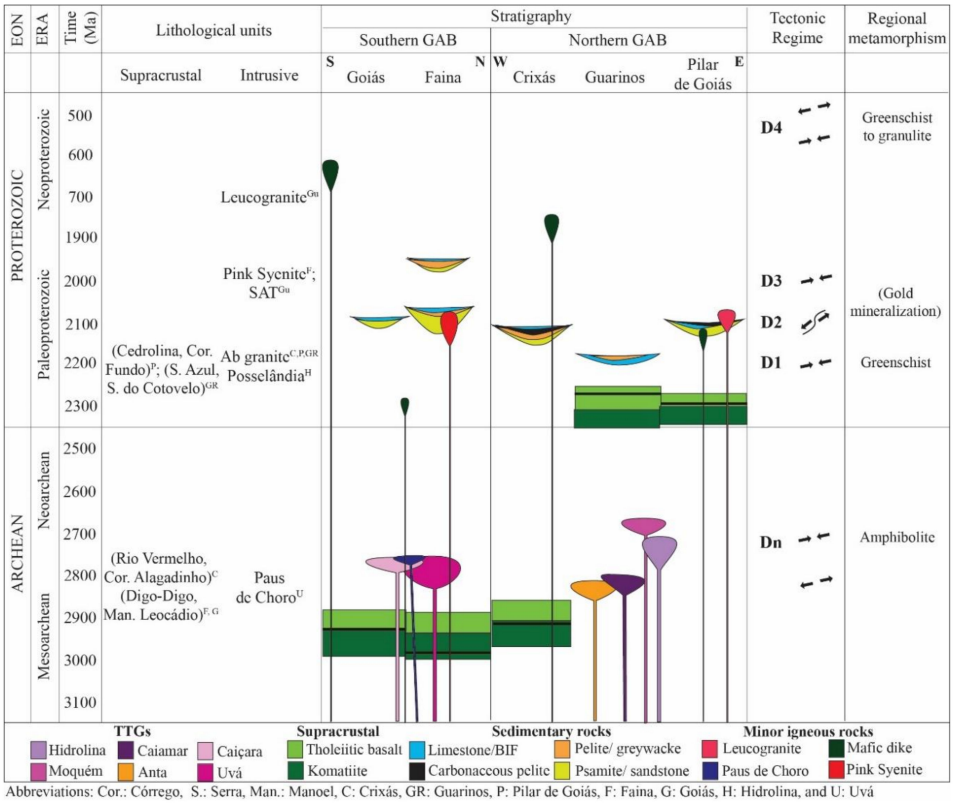

Figure 2. Stratigraphic columns for the greenstone belts in the northern and southern Goiás Archean Block (GAB). Age compilation for greenstone belts according to [11,18,71,77,82,83]. Age references for the TTGs based on [11,22,24,25,72] and this work.

All greenstone belts of the GAB were initially interpreted as synformal keels based on their geometry and lithostratigraphy [71]. However, this is currently accepted only for the two southern greenstone belts [82], whereas the northern greenstone belts are interpreted as fold-thrust belts [71]. Overall, the greenstone belts display a similar sequence of lower komatiite (400–900 m) followed by tholeiitic basalt flows (300–500 m) [71]. Primary volcanic features such as spinifex and/or cumulatic textures are locally preserved in ultramafic rocks [84–86]. Basaltic flows are characterized by pillow and variolitic structures with local dolerite and gabbro dikes/sills [71]. Minor BIF, gondite and/or chert lenses occur as thin layers intercalated with volcanic rocks [71,82]. The transition from lower volcanic to upper sedimentary rocks is typically marked by a tectonic unconformity. In the Faina and Goiás greenstone belts, the volcanic sequences have a maximum depositional age approximately between 2960 and 2920 Ma according to zircon U-Pb LA-ICP-MS geochronology [77], whereas in Crixás the maximum depositional age is indicated by Sm-Nd whole-rock isochron age of ca. 3000 Ma [87]. In contrast, the other two greenstone belts were formed during the Paleoproterozoic. In the Guarinos greenstone belt, lower volcanic rocks are dated at 2180 Ma [76], whereas in the Pilar de Goiás greenstone belt, volcanism is dated at 2165 Ma [11].

Unlike the lower mafic-ultramafic sequences, the overlying sedimentary units of the five greenstone belts indicate diverse depositional environments [18,82]. At Crixás, initial sedimentation is represented by carbonaceous schists typical of euxinic environments, with oolitic to stromatolitic marbles of dolomitic composition that are unconformably overlain by pelites and greywackes [88]. At Guarinos, lower chlorite-rich pelites containing clasts of basalt are laterally interlayered with basalts that are overlain by chemical sedimentary rocks (BIF, chert), conglomerate lenses and pelites [71,89,90]. At Pilar de Goiás, calcsilicate rocks, sandstone and dolomite are followed by greywackes [20].

The stratigraphy of the two southern greenstone belts was initially proposed by Danni et al. [91] as a single greenstone belt composed of lower volcano-sedimentary sequence unconformably overlain by upper sedimentary rocks. Due to their contrasting characteristics, Teixeira [92] subdivided this belt into the Faina and Goiás greenstone belts with lower komatiitic, basaltic and felsic volcanic rocks and upper siliciclastic, pelitic and chemical sedimentary rocks. The Goiás greenstone belt (previously known as Serra de Santa Rita) is characterized by lower carbonaceous-rich pelites followed by chert, BIF, and dolomite unconformably overlain by turbidites [93]. The Faina greenstone belt is characterized by two sequences consisting of lower conglomerate, quartzite and pelite overlain by chemically precipitated rocks [93].

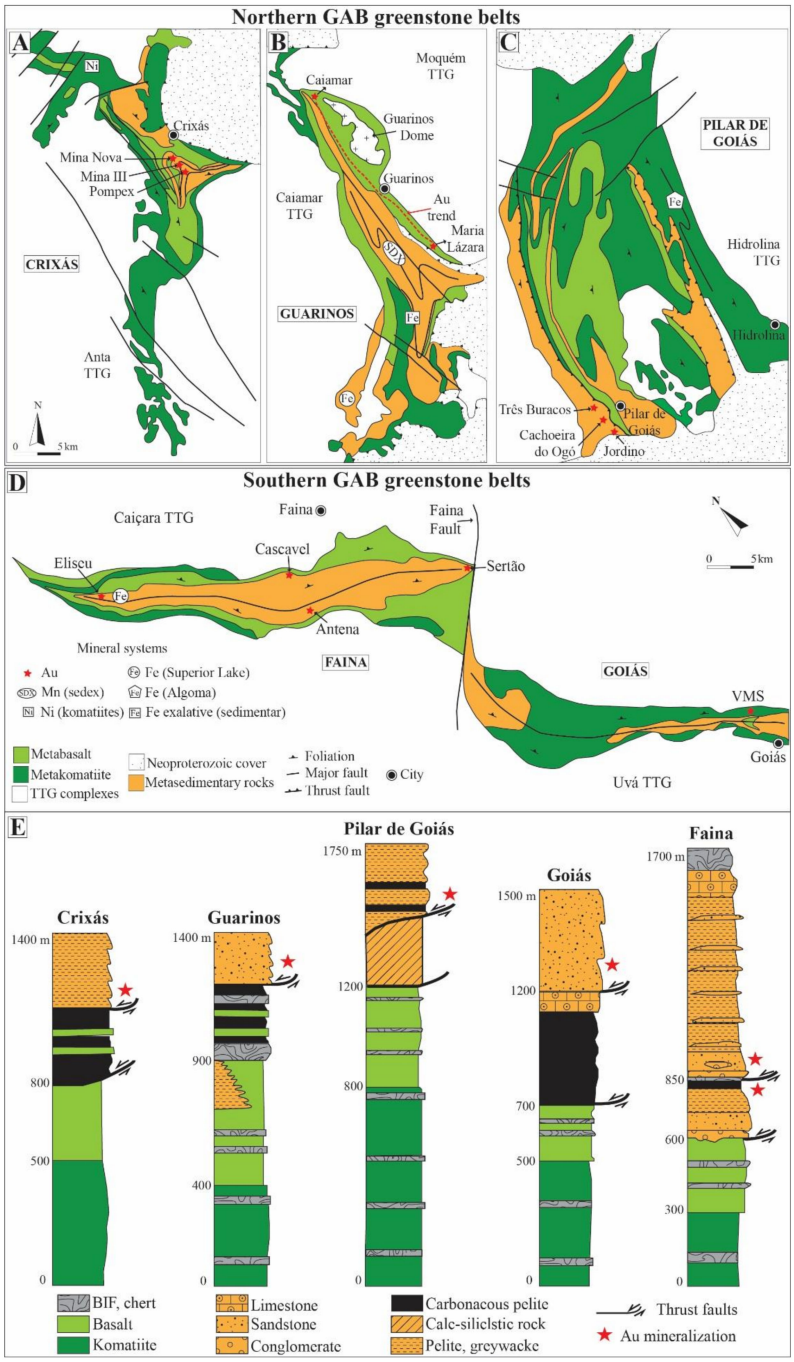

Figure 3. Geology of northern (**A**–**C**) and southern (**D**) greenstone belts from the Goiás Archean Block (GAB), with corresponding stratigraphy (**E**).

The maximum deposition age of sedimentary rocks for all greenstone belts is constrained by a mafic dike swarm emplaced between 2500–2300 Ma [94] that crosscuts Archean TTG complexes and volcanic rocks from the Goiás, Faina and Goiás belts (but not their upper sedimentary rocks). This field relationship implies that the sedimentary rocks must have been deposited following or during regional crustal extension after 2300 Ma. The end of sedimentation is indirectly constrained by carbon isotopes of upper dolomitic rocks [75,82,95,96]. This was based on chemostratigraphic markers that reflect the oxidation of the atmosphere in the Paleoproterozoic known as the Jatuli event [97]. Upper dolomites from the northern greenstone belts and the lower sedimentary sequence from the southern greenstone belts show positive $\delta^{13}C$ values (+10‰ to +14‰) that coupled with available geochronology indicate their deposition between 2220–2060 Ma [15,96], marking the first carbon anomaly of the Jatuli event following glaciation in the Huronian. Moreover, upper dolomites from the second sedimentary cycle of Faina and Goiás greenstone belts record mixed $\delta^{13}C$ values (−0.66‰ to +0.66‰), which suggest their deposition at the end of Jatuli event, late in Rhyacian times and likely associated with extension in early Orosian [71].

Deformation History

The GAB shows a polyphase evolution recorded by complex deformation patterns [12]. This complexity, together with the lack of absolute dating of regional structures, has hindered a better understanding of the deformation history of the GAB, as indicated by previous studies published in the region [72,98–100]. Early structural interpretations are reconsidered based on most recent geochronology and isotope geochemistry data including new data presented herein. At least three deformation events in the GAB were developed in the Archean, Paleoproterozoic, and Neoproterozoic (Table 2). These deformation events are recorded by titanite U-Pb SHRIMP dating of the Crixás Açu gneiss, which revealed distinct metamorphic episodes at 2711 Ma, 2011 Ma and 590 Ma [21,101].

The Archean Dn event was responsible for regional amphibolite facies metamorphism and deformation of all granite-gneiss TTG complexes and lower volcanic sequences of the Crixás, Faina and Goiás greenstone belts [77,87]. Structures formed during Dn include tight to isoclinal folds, thrust faults and metamorphic foliation (Sn). The amphibolite facies metamorphism is expressed by talc-serpentine-chlorite ± titanite and quartz-hornblende-biotite-epidote-titanite parallel to Sn in the volcanic rocks and TTG granite-gneisses, respectively [99,102]. The contacts with adjacent granite-gneiss TTG complexes are commonly marked by deformed xenoliths of volcanic rocks in the southern belts, which suggest the greenstone belts are allochthonous [77,93]. In the northern GAB, an Archean metamorphic event, registered at ~2700 Ma, is coeval with the emplacement of younger orthogneisses [21], whereas in the southern GAB metamorphism is dated at ca. 2840 Ma [25]. The minimum age of the Dn event is provided by NE- and NW-trending mafic dikes dated by Rb-Sr (whole rock) and $^{40}Ar/^{39}Ar$ (hornblende) to 2490 ± 40 Ma, which crosscut the TTG complexes and lower volcanic rocks in the Faina, Goiás and Crixás greenstone belts [94].

In the Paleoproterozoic, D1, D2, and D3 brittle-ductile events comprise regional deformation, metamorphism and gold mineralization hosted in greenstone belts of the GAB. Early developed structures include S1 foliation developed parallel to subparallel to the bedding (S0), axial planar to tight to isoclinal folds and the inversion of the stratigraphy in the greenstone belt sequences [93,103,104]. Regional metamorphism comprises quartz-chlorite-muscovite-biotite ± epidote assemblages oriented parallel to S1 foliation in the volcano-sedimentary rocks of the greenstone belts. This assemblage is compatible with greenschist to lower amphibolite facies and temperature ranges that roughly correspond to the brittle-ductile transition [105]. Gold mineralization is associated with D2 thrust faults and, to a minor extent, D3 shear zones. The Au-related hydrothermal assemblages in all deposits overprint greenschist facies metamorphic assemblages and therefore post-date peak metamorphism [12,106].

Table 2. Previous deformation history of the GAB.

Reference	Event	Timing	Structural Features	Description
Danni et al., [67]	D1	Archean	Subtly W-dipping S1 foliation axial planar to isoclinal (-tight) F1 folds	Greenschist facies metamorphism. Stratigraphic inversion.
	D2	Archean	Subtly to moderate W-dipping S2 foliation axial planar to isoclinal F2 folds	Late mafic dike and granitic intrusions.
Queiroz, [59]	Dn−3	Archean	Sn−3//So	Basin closure and orogen development. Inherited zircon xenocrysts of juvenile nature. Stratigraphic inversion of supracrustal sequences.
	Dn−2	Archean	Sn−2	Polydiapiric, juvenile magmatism at 2840 [A], 2820 [B], and 2880 [C] Ma, followed by 2700 [D] Ma crustal-derived granite and granodiorite intrusions in the Moquém terrane. Dome-and-keel structure; amphibolite facies metamorphism.
	Dn−1	Paleoproterozoic	Subtly S-dipping Sn−1 foliation and sub-horizontal W-plunging mineral lineation; tight to isoclinal N-striking folds	Transpression resulted in N30° W dextral displacement (e.g., Engenho Velho shear zone) and N30° E sinistral shear faults.
	Dn Dn+1	Neo-proterozoic	Subtly S-dipping Sn foliation and W-plunging mineral lineation; displacement towards the SE direction	Amalgamation of the GAB into the Brasília Fold Belt during closure of the Goianides ocean (Western Gondwana).
Jost and Fortes, [12]	D1	Archean	S1//S0	Regional greenschist facies metamorphism. Stratigraphic inversion of supracrustal sequences.
	D2	Archean	No structural data.	Emplacement of the Anta, Caiamar, and Hidrolina terranes.
	D3	Paleo-proterozoic	S1//S0; isoclinal folds	Late magmatic activity (mafic dikes and granitic intrusions).
	D4	Neo-proterozoic	Reorientation of D3 folds	Deformation decreases from W to E.
This work	Dn	Archean	Moderately NE- to NW-dipping Sn foliation and local N-verging open folds	Greenstone belt volcanism (Crixás, Faina, and Goiás greenstone belts) and TTG plutonism. Amphibolite facies metamorphism.
	D1	Paleo-proterozoic	Subtly NW- to W-dipping S1 foliation, axial planar to sub-horizontal NW-striking isoclinal folds	Stratigraphic inversion; greenschist facies metamorphism.
	D2		Subtly W- to NW-dipping S2 foliation, axial planar to sub-horizontal NW-striking isoclinal folds	Stacked early formed thrust faults; Main gold mineralization event.
	D3		Moderately W- to NW-dipping S3 foliation, local N-striking open folds, NW-striking shear zones, gently S-dipping thrust faults	Minor granitic (±mafic) magmatism in supracrustal sequences; Minor gold mineralization.
	D4	Neo-proterozoic	Steeply/moderately S- to W-dipping normal faults; sub-horizontal and steeply S-plunging slicken lines, respectively	Incorporation of the GAB in the Brasília Fold Belt during the Brasiliano orogen. Regional granitic magmatism and amphibolite facies metamorphism.

[A]: 2840 Ma event represented by the Tocambira tonalite (2842 ± 6 Ma, εNd = +2.4) and Águas Claras gneiss (2844 ± 7 Ma, εNd = −0.6) in the Caiamar terrane. [B]: 2820 Ma event represented by granodiorite (2820 ± 6 Ma, εNd = + 0.1) in the Anta terrane, Crixás-Açu gneiss (2817 ± 9 Ma, εNd = +0.6) in the Caiamar terrane. [C]: 2880 Ma event represented by granite (2792 ± 7 Ma, εNd = 0.0) in the Anta terrane and granodiorite (2844 ± 7 Ma; no εNd data) in the Hidrolina terrane. [D]: ~2700 Ma event represented by granite (2711 ± 3 Ma, εNd = −2.0) and granodiorite (2707 ± 4 Ma, εNd = −2.2) in the Moquém terrane.

Contrasting structural evolution is recorded in the northern and southern greenstone belts for the Paleoproterozoic D1, D2 and D3 events (Table 3). In greenstone belts of the northern GAB, structures developed throughout these events include: (i) subtly ~ W-dipping S1 foliation (S0 transposed into S1), subtly W-dipping, NS-trending thrust faults, greenschist faces metamorphism and stratigraphic inversion; (ii) subtly S-dipping S2 foliation, planar axial to isoclinal F2 folds, local mm- to cm-wide shear zones, subtly N-dipping, EW-trending thrust faults and stacking of the stratigraphy; (iii) subtly E-dipping S3 foliation, subtly E-dipping, NS-trending F3 folds and lateral thrust ramps [99,103,107,108]. In the southern GAB, Paleoproterozoic deformation is largely described based on observations in the Faina greenstone belt [106]. The D1 event is expressed by moderately N-dipping S1 foliation (S0 transposed into S1), subtly W-dipping, NNW-trending F1 folds, stratigraphic inversion and greenschist facies metamorphism. The D2 event is characterized by subtly S-dipping S2 foliation, planar axial to tight to isoclinal F2 folds, gently W-plunging mineral lineation, gently S-dipping, and EW-trending thrust faults that caused stacking of the stratigraphy. The D3 event is represented by moderately N-dipping S3 foliation, NW-trending, S-dipping shear zones and subtly S-dipping thrust faults. Significant hydrothermal fluid flow along D2-related structures resulted in the development of Au-bearing quartz ± carbonate veins with only localized hydrothermal fluid flow produced during a D3 event.

Table 3. Deformation events proposed for the GAB.

Event	Stress Field	Description		Au Endowment
		Northern Greenstone Belts	Southern Greenstone Belts	
D1		~EW shortening; subtly ~ W-dipping S1 foliation (//S0); subtly W-dipping, NS-trending thrust faults; greenschist facies metamorphism; stratigraphic inversion.	~EW shortening; moderately N-dipping S1 foliation (//S0); subtly W-dipping, NNW-trending F1 folds; greenschist facies metamorphism; stratigraphic inversion.	barren
D2	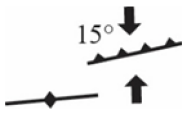	~NS shortening; subtly S-dipping S2 foliation, planar axial to isoclinal F2 folds; subtly N-dipping, EW-trending thrust faults; local mm- to cm-wide shear zones; stacking of stratigraphy.	~NNW-SSE shortening; subtly S-dipping S2 foliation, planar axial to tight to isoclinal F2 folds; gently W-plunging mineral lineation; EW-trending, gently S-dipping thrust faults; stacking of stratigraphy.	Au
D3	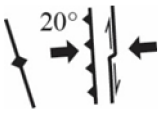	~EW shortening; subtly E-dipping S3 foliation; subtly E-dipping, NS-trending F3 folds; lateral/frontal thrust ramps.	NE-SW shortening; NW-trending shear zones; moderately N-dipping S3 foliation; subtly S-dipping thrust faults.	(±Au)
D4	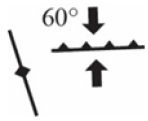	~NNW-SSE to EW shortening; steeply W-dipping, local NNW-trending F4 folds.	NS to EW shortening; moderately S-dipping faults, gently S-plunging slicken lines; steeply W-dipping faults, steeply S-plunging slicken lines; fault-fill veins and breccias.	barren (?)
References		[86,90,94,95]	[12,69,93]	

The timing of Paleoproterozoic deformation represented by D1 to D3 events can be stipulated by a series of intrusions emplaced between ~2170 and 2061 Ma. Early deformation is constrained by intrusion of the Posselândia diorite along the N-trending shear zone that crosscuts the Hidrolina TTG terrane and has a zircon U-Pb SHRIMP age of 2146 ± 2 Ma [109]. Mafic dikes crosscutting Au-related hydrothermal alteration in metasedimentary rocks from the Crixás greenstone belt show zircon U-Pb LA-ICP-MS age of 2170 ± 17 Ma [74]. Syntectonic granites within N-verging thrust faults in the Pilar de Goiás greenstone belt yield a zircon U-Pb SHRIMP age of 2145 ± 12 Ma [72,110]. The lower limit of the Paleoproterozoic deformation is constrained by syn- to late-tectonic Pink Syenite intrusion in the Faina greenstone belt with zircon U-Pb SHRIMP age of 2061 ± 14 Ma (Results section).

The Neoproterozoic D4 event overprints, offsets and/or reactivates previous structures. Structural features developed in D4 include subtly S- to W-plunging crenulation lineations associated with thin-skinned, E-verging thrust to reverse faults and local NS-trending open folds [111]. This event is attributed to the Brasiliano/Pan-African orogeny at 650–480 Ma [112]. The timing of D4 is indirectly constrained by isotopic disturbance, e.g., Pb loss and lower concordia intercepts at approximately 600 Ma in zircon U-Pb geochronology ([21,22,28] and this work). The maximum age range of the D4 event is constrained by a leucogranite intrusion in the Guarinos greenstone belt with U-Pb LA-ICP-MS age on hydrothermal zircon of 729 ± 15 Ma [10]. The minimum age range of this event is ascertained by the Serra Negra intrusion at the western border of the GAB with a zircon U-Pb SHRIMP age of 527 ± 5 Ma (Results section).

5. Gold in the Goiás Archean Block

The mineral systems of the GAB are dominated by orogenic gold deposits hosted in greenstone belts with poorly described paleoplacer and intrusion-related gold showings. Additional mineral systems recognized (but not currently economic) include minor Algoma and superior-type Fe ore, sedimentary-hosted Mn, and Au ± Cu VMS [11]. The gold deposits hosted in greenstone belts share many similarities, e.g., strong structural control, metal association, hydrothermal alteration and mineralogy, with orogenic gold deposits worldwide [113,114]. This section presents a summary of pertinent structural, mineralogical, hydrothermal alteration, ore assemblage characteristics and hydrothermal fluid conditions of significant orogenic gold deposits and occurrences in the GAB.

5.1. Deposit Structural Controls

The location of the gold deposits and the geometry of the ore shoots display strong structural control, with mineralization typically hosted in intensely deformed zones associated with shear zones [12,95]. At the regional and camp scales, high-grade gold deposits (>2 g/t Au) are spatially associated with thrust and/or strike-slip faults, ductile-brittle shear zones and folds developed during D2 (-D3) deformation events. These structures are commonly located parallel to lithological contacts such as those between the volcano-sedimentary sequences and the surrounding TTG complexes [12]. In the northern portion of the GAB, ore bodies relate to, and are controlled by, D2 thrust faults that consistently verge to the east, dextral strike-slip faults (e.g., Engenho Velho and Faina, in the Guarinos and Faina greenstone belts, respectively), and sinistral strike-slip faults (e.g., Cachoeira do Ogó, in the Pilar de Goiás greenstone belt) [12]. At a deposit scale, ore shoots typically comprise elongated (up to 1500 m) bodies with down-plunge continuity parallel to a prominent stretching lineation developed in hydrothermal minerals and are particularly developed along high-strain shear zones [12,95]. Another important control on high-grade ore shoots is illustrated by the intersection of fault zones or shear zone planes with the dip of metamorphosed volcanic or sedimentary rocks. Where the fault zone or shear zone crosscuts chemically favourable units, e.g., carbonaceous schist and BIF (Mina Nova and Sertão deposits in the Crixás and Faina greenstone belts, respectively), massive replacement ore bodies along strike of these rocks display an apparent stratabound mineralization style [12].

5.2. Hydrothermal Alteration and Mineralization Styles

Hydrothermal alteration zones associated with Au mineralization in the GAB indicate enrichment in SiO_2, CO_2, K_2O and S [12]. Major controls on hydrothermal alteration include host rock chemistry, structural setting, the fluid/rock ratio, and permeability during deformation. The gold-related hydrothermal alteration typically overprints metamorphic assemblages, but the distinction between regional metamorphic host rocks and distal alteration can be subtle. Three major mineralization styles are observed in the GAB: disseminated sulfide, vein-hosted and massive sulfide (Figure 4 and Table 4). Most deposits are associated with a single style of mineralization, although some contain more than one style (e.g., Mina III and Sertão).

Table 4. Mineralization styles of orogenic gold deposits in the GAB.

Mineralization Style	Characteristics	Host Rocks	Hydrothermal Alteration	Metal Association	Deposit
Disseminate sulfide	Stratabound replacement of Fe-rich host rocks by pyrite, arsenopyrite, chalcopyrite, and pyrrhotite. Often associated with quartz ± carbonate veins	BIF, dolomite marble ± carbonaceous schist	white mica-pyrite-arsenopyrite-chalcopyrite-pyrrhotite	Au-Ag-As ± Cu	Mina Nova/Forquilha (Crixás); Três Buracos/Ogó/Jordino (Pilar de Goiás); Sertão (Faina), Maria Lázara (Guarinos)
Vein-hosted	Quartz ± carbonate ± tourmaline ± albite/K-feldspar veins. Vein types include shear, laminated, and fault-fill. Sulfides minerals include pyrite, chalcopyrite, and arsenopyrite.	quartzite, carbonaceous schist ± BIF	quartz-white mica ± fuchsitic mica ± biotite ± pyrite-chalcopyrite	Au-Ag ± Pb	Mina III (Crixás), Cascavel (Faina)
Massive sulfide	Semi- to massive lenses with pyrrhotite, arsenopyrite, chalcopyrite, pyrite with minor bornite and galena.	metabasalt, carbonaceous schist ± BIF	white mica-quartz ± chlorite ± biotite ± garnet ± tourmaline	Au-Ag-As-Pb ± Sb	Mina III (Crixás), Sertão (Faina)

Disseminated sulfide is the most common mineralization style observed in the Crixás, Guarinos, Pilar de Goiás and Faina greenstone belts. It comprises disseminated pyrrhotite-arsenopyrite-pyrite ± chalcopyrite in 0.1 to 5 m-wide proximal alteration zones surrounding quartz ± carbonate veins (e.g., Mina Nova). This mineralization style consists of 1.5 m wide, 200 m long orebodies that extend up to 1000 m down plunge. It is developed in hydrothermally altered wall rock associated with ductile shear zones, typically hosted by carbonaceous schists, metavolcanic and metasedimentary Fe-rich rocks. The hydrothermal alteration consists of white mica-quartz-ankerite/siderite ± chlorite assemblages, with minor albite ± K-feldspar and associated quartz ± ankerite/siderite veins. At Sertão, proximal white mica-K-feldspar-pyrite-chalcopyrite alteration zone shows poikiloblastic textures that suggest replacement of Fe-rich carbonates by sulphides (Figure 5). Gold (≤50 μm) is in equilibrium with pyrrhotite (e.g., Maria Lázara) and arsenopyrite (e.g., Sertão, Jordino, and Ogó), or as inclusions and fracture-fills within these sulphides, with rare free gold (≤30 μm) in both quartz veins and proximal alteration assemblages. The approximated gold fineness associated with this style of mineralization is 920 [106,107]. At the Crixás deposits, estimated production of 3 Mt of ore is reported with an average of 6 g/t Au [12], whereas at the Sertão deposit, oxidized sulfide-rich ore resulted in 256 Koz at 24.95 g/t [115].

Massive sulfide consists of 0.5–2.5 m wide, 50–200 m long foliation-parallel, sulfide-rich orebodies. This mineralization style is developed adjacent to the contact between metabasalts and carbonaceous schists, e.g., in the Palmeiras and Zona Superior orebodies of the Serra Grande Mine [95,116]. At the Zona Superior orebody, massive sulfide lenses extend up to 200 m down-plunge, with an estimated production of 2 Mt at 12 g/t Au for deposits in the Crixás greenstone belt [12]. Sulfides (up to 95 vol.%) include massive pyrrhotite and/or arsenopyrite, with subordinated magnetite, bornite, chalcopyrite, and ilmenite [11]. Gold (0.1–2 mm) is distributed as irregular grains with an approximated fineness of 900 [95,117]. In the Faina greenstone belt, minor stratabound-like, massive sulfide mineralization is associated with chemically reactive host rocks such as BIF, e.g., at Sertão. In this deposit, pervasive replacement of Fe-rich carbonates (Fe-dolomite, ankerite, and siderite) by Fe-sulphides is observed [106].

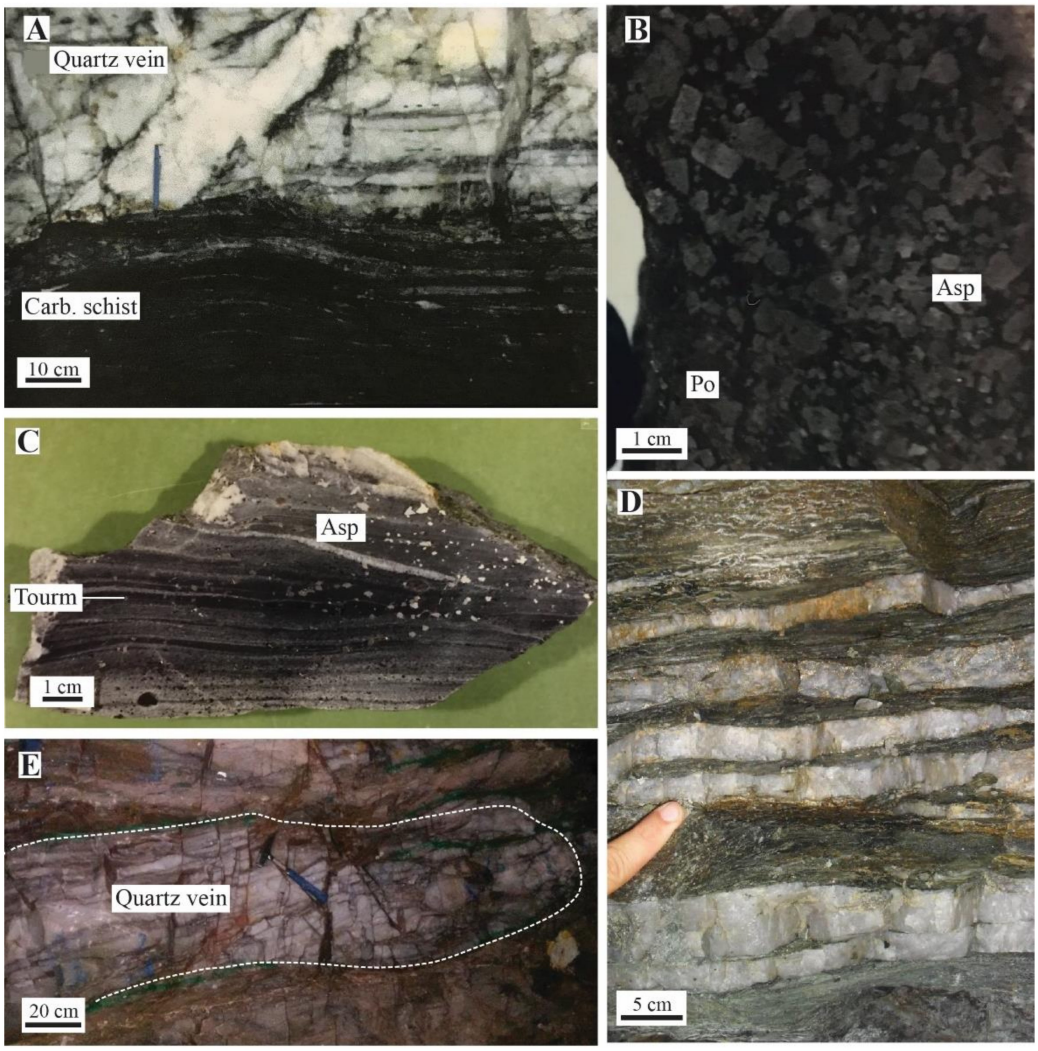

Figure 4. Hand samples showing mineralization styles in orogenic gold deposits of the GAB. (**A**) Vein-hosted [118] and (**B**) massive sulfide [119] mineralization in carbonaceous schist of the Mina III orebody; (**C**) disseminated sulphides in the Maria Lázara deposit. Note Asp overprints Wm-Tour hydrothermal assemblage [14]; (**D**) laminated quartz veins and gold disseminated in Py-Asp-Po from the Ogó deposit (Pilar de Goiás) [120], and (**E**) vein-hosted mineralization controlled by isoclinal F2 folds in the Pilar mine [120]. Abbreviations correspond to Ank: ankerite, Asp: arsenopyrite, Py: pyrite, Po: pyrrhotite, Sid: siderite, Wm: white mica.

Vein-hosted ore consists of deformed quartz ± carbonate veins locally hosted in shear zones. It forms 0.5–2 m wide, 500 m long, 1500 m down-dip orebodies that record an estimated production of 3 Mt at 8 g/t Au for deposits in the Crixás greenstone belt [12]. Despite the lack of an available ore reserve associated with this mineralization style in the Faina greenstone belt, V2 veins in the Cascavel deposit record grades of up to 4 g/t [121]. This type of mineralization is hosted by carbonaceous schist and quartzite in the Crixás and Faina greenstone belts, respectively. At the Crixás deposits (e.g., Mina III), typical white mica-carbonate-chlorite-pyrrhotite-arsenopyrite assemblages enveloping D2-related veins contain free gold (0.1–2 mm) with a fineness of 910 [12]. At Cascavel, proximal white mica-quartz ± pyrite ± chalcopyrite alteration zones developed around V2 veins display free gold (≤250 mm) with a fineness of 992 [106].

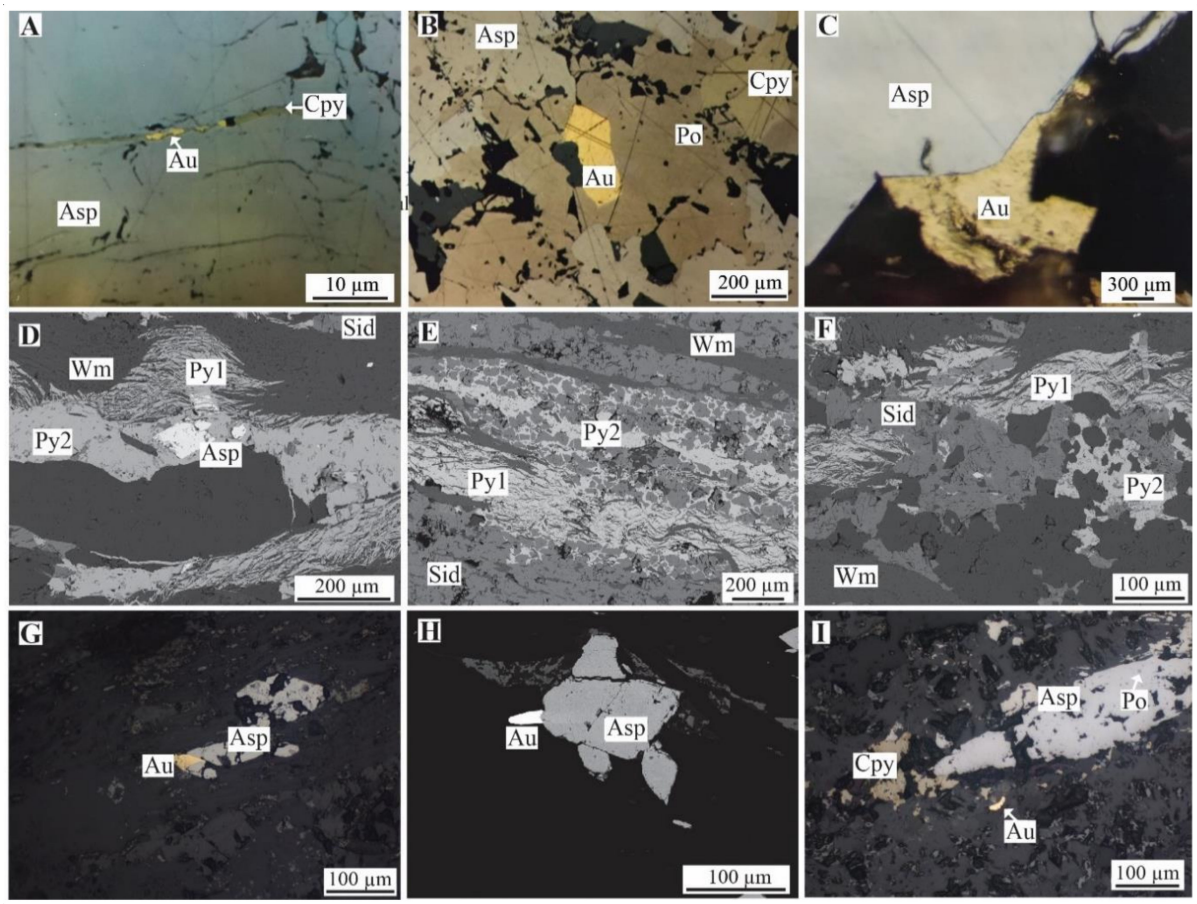

Figure 5. Photomicrographs showing ore assemblage, mode of occurrence and distribution of gold in the GAB deposits. (**A**) Gold and Cpy filling microfracture in Asp of massive sulfide ore in Mina III deposit [119]; (**B**) gold (≤200 µm) with Po-Cpy-Asp of massive sulfide from Mina III deposit [119]; (**C**) native Au bordering Asp from disseminated mineralization in the Maria Lázara deposit. Dissolution microcavities in gold grains suggest remobilization processes [14]; (**D**) idiomorphic Asp overprinting sulphides (Py1 and Py2) in proximal BIF at the Sertão deposit [106]; (**E**) textural contrast of fine-grained, deformed Py1 and coarse-grained, poikiloblastic Py2 after replacement of ankerite/siderite in proximal BIF at the Sertão deposit [106]; (**F**) siderite overprinting Py1 and being replaced by Py2 in BIF at the Sertão deposit [106]; (**G**) gold (≤50 µm) in equilibrium with Asp shows microfractures and dissolution features in proximal carbonaceous schist at the Sertão deposit; (**H**) BSE image of elongated Au (ca. 30 µm) in equilibrium with Asp with pressure shadows filled by white mica in proximal carbonaceous schist at the Sertão deposit [106], and (**I**) free Au (ca. 20 µm) adjacent to subhedral Asp-Py-Cpy in BIF at the Sertão deposit [106]. Abbreviations correspond to Asp: arsenopyrite, Cpy: chalcopyrite, Py: pyrite, Po: pyrrhotite, Sid: siderite, Au: gold, Wm: white mica.

5.3. Fluid Conditions

Few available studies have focused on the conditions of ore-related fluids of orogenic gold deposits in the GAB [14,95,107,122]. Fluid inclusions in quartz from disseminated massive sulfide ore in the Mina III deposit, at the Crixás greenstone belt, show highly saline fluids in the H_2O-CO_2-NaCl-KCl-CH_4-N_2 system [95]. However, quartz from vein-hosted ore also from Mina III are characterized by (i) predominant low salinity (< 10 wt. % NaCl eq.), H_2O-CO_2-rich fluids, and (ii) subordinate saline (>8 wt. % NaCl eq.), H_2O-CO_2-rich fluids enriched in CH_4, N_2 with rare methane- and nitrogen-rich inclusions [95]. Based on fluid inclusion homogenization temperatures, the Mina III deposits were formed between 350 to 475 °C, and at pressures of 2–3 kbars [95]. Additional garnet-biotite geothermobarometry and fluid inclusion analysis in quartz from disseminated and vein-hosted mineralization styles of Orebodies IV and V in the Crixás greenstone belt indicate temperatures from 428 to 580 °C, and pressures of 5.7 to 8.3 kbars [107]. The high-pressure

conditions obtained by Petersen Jr. [107] are interpreted to reflect increased crustal depth at the time of mineralization. The temperature range for the formation of these deposits is comparable with greenschist to lower amphibolite facies. Additional estimates of fluid conditions for deposits hosted in other greenstone belts in the northern GAB include studies by Pulz [14,122] at the Maria Lázara and Cachoeira do Ogó deposits, in the Guarinos and Pilar de Goiás greenstone belts, respectively. According to these studies, temperature ranges from 335 to 450 °C and pressure from 2 to 3 kbars are associated with hydrothermal fluids in these deposits. In the Faina greenstone belt, chlorite and arsenopyrite geothermometry suggest temperatures of 330–400 °C and 320–430 °C for the Cascavel and Sertão deposits, respectively [106]. Thus, the deposits of the GAB have estimated fluid temperatures and hydrothermal alteration assemblages (Table 5) comparable with other mesothermal greenstone-hosted orogenic gold deposits worldwide [1,13].

The transport and precipitation of gold in orogenic Au deposits of the GAB is interpreted to have occurred by several different mechanisms, as evidenced by contrasting occurrence and composition of gold. Major controls include destabilization of sulfide and chloride complexes, phase immiscibility and variations in pH and fO_2. Mineralization during episodic flow of hydrothermal fluids (e.g., [123]) is widely attributed to gold deposits in the GAB. Evidence for the multistage precipitation of ore-related minerals is illustrated by (i) distinct paragenetic generation of ore-related mineral phases, (ii) contrasting Ag contents of gold (e.g., Maria Lázara deposit; [124]), (iii) free and refractory gold (e.g., Cascavel and Sertão deposits; [106]), (iv) crack-and-seal textures in vein-hosted mineralization (e.g., [14]), and (v) dissolution of ore-related minerals such as arsenopyrite (e.g., [122]).

Table 5. Summary of characteristics of orogenic gold deposits in the GAB.

Greenstone Belt	Faina		Crixás		Pilar de Goiás	Guarinos
Deposit	Sertão	Cascavel	Mina III	Corpos III & IV	Ogó/Jordino/Três Buracos	Maria Lázara
Host rock	carbonaceous schist and BIF	quartzite and biotite schist	carbonaceous schist, metabasalt, and marble		carbonaceous schist and metabasalt	
Metamorphic grade	Greenschist		Greenschist to lower amphibolite		Greenschist	
Structural controls	gently S-plunging fold hinges; EW-trending, subtly S-dipping thrust faults; subtly NW-trending shear zones		gently N-plunging fold hinges; EW-trending, subtly N-dipping thrust faults		gently W-plunging fold hinges; NS-trending, subtly W-dipping thrust faults	steeply S-dipping foliation; NW-trending, steeply SE-dipping shear zones
Mineralization style	disseminated sulphides (± vein, massive sulfide)	vein-hosted (± disseminated sulphides)	disseminated sulphides (± vein-hosted)	disseminated sulphides	vein-hosted and disseminated sulphides	
Ore assemblage	Qtz-Ank/Sid-Asp-Py ± Cpy ± Po	Qtz ± KF-Au ± Py ± Cpy	Chl-Grt-Po-Asp	Au-As-Ag (±Cpy ± Bn ± Pent)	Asp-Py-Po-Sph-Gn-Cpy	Asp-Po ± Sph ± Py± Cpy ± Gn ± Mo ± Ag (late Au-Te-Bi)
Au endowment	256 Koz., 24.95 g/t (Troy Resources)	No data	7.3 Moz, 10 g/t (AngloGold)		2.3 Moz, 4 g/t (Yamana Gold)	4.22 Moz, 4 g/t (Yamana Gold)
Geochemical signature	Au-Ag-As-Sb-Pb ± Cu	Au-Pb ± As ± Sb	Au-As		Au-Ag-Bi-Mo-Pb-Sb-W	Au-Ag-Sb (main) Au-Te-Bi (late)
Mineralization age	No data		2126 ± 16 Ma (arsenopyrite Re-Os; [[])		2025 Ma (galena Pb-Pb; [[])	No data
Au fineness	~945	~992	~944	~915	No data	~920
Temperature	320–430 °C	310–420 °C	No data	428–580 °C	335–450 °C	330–450 °C (main event) 116–241 °C (late event)
References	[106]		[107,119,125,126]		[14,122,127]	

Abbreviations: Qtz: quartz, Bt: biotite, Chl: chlorite, KF: alkali-feldspar, Grt: garnet, Ank: ankerite, Sid: siderite, Py: pyrite, Cpy: chalcopyrite, Gn: galena, Po: pyrrhotite, Asp: arsenopyrite, Mo: molybdenite, Sph: sphalerite, Te: tellurium, Bi: bismuth, Bn: bornite, Au: gold, Ag: silver.

In several deposits, including Cachoeira do Ogó and Cascavel in the Pilar de Goiás and Faina greenstone belt, gold occurs as free grains in quartz veins, indicating the involvement of contrasting ore-forming processes. The deposition of free gold in D_2-related veins at the Cachoeira do Ogó and Cascavel deposits is possibly caused by fluid immiscibility (or boiling) and subsequent lowering of the gold solubility [128,129]. The cause of fluid immiscibility in Au-bearing veins associated with D2 thrust faults is attributed to cyclic decompression of the hydrothermal fluid caused by seismic movement along the thrust faults and veins [130–132]. In this scenario, gold transport involving vein-hosted mineralization styles would be facilitated via chloride complexes (e.g., [106]).

5.4. Timing of Au Mineralization

The timing of the gold mineralization event in the GAB is a matter of contention [16,95,125]. Based on the estimated age of greenstone belts, gold mineralization was initially interpreted to be Archean [80]. Subsequent studies proposed that massive sulfide orebodies in the Crixás greenstone belt (CGB) formed post-peak metamorphism associated with the Brasiliano orogeny [125]. Neoproterozoic ages for gold mineralization were reinforced by K-Ar and Ar-Ar ages from amphibole at 660–730 Ma, biotite and chloritoid at 520–580 Ma, and biotite and muscovite at ~500 Ma [133], together with a whole-rock Rb-Sr isochron of Au-bearing chlorite-garnet schist at 505 ± 7 Ma [87]. However, ages obtained from these methods are easily disturbed by subsequent thermal events and thus considered unreliable to constrain ages within polymetamorphic terranes such as the GAB [21,22].

Additional geochronological data for the gold mineralization event in the GAB is offered by more recent studies [16,72,122,134]. Arsenopyrite Re-Os of massive sulfide from the Mina III deposit in the Crixás greenstone belt is dated at 2126 ± 16 Ma [16]. In the Pilar de Goiás greenstone belt, galena Pb-Pb model age of 2025 Ma [122] gives a robust, but imprecise estimate of gold mineralization. The latter is refined by zircon U-Pb SHRIMP age of 2145 ± 12 Ma for syn-tectonic albite granite intrusion in the same belt [72]. The previous data is consistent with U-Pb SHRIMP age of 2165 ± 47 Ma obtained for hydrothermal zircon hosted in mineralized metagreywacke [134]. Therefore, a Paleoproterozoic age is presumed for the gold mineralization event in the GAB.

In the Faina greenstone belt, the maximum age of gold mineralization is indirectly constrained by 2061 Ma Pink Syenite intrusion synchronous with the Au-related deformation event (Results section). The minimum age of gold mineralization is constrained by evidence from paleoplacer deposit in basal meta-conglomerate of the Faina greenstone belt [135]. The presence of deformed clasts of Au-bearing quartz-veins, disseminated sulphides in carbonaceous schist, and gold within a fine-grained matrix suggest the paleoplacer post-dates the main Au-related hydrothermal event [135]. This is consistent with other Paleoproterozoic paleoplacer deposits, such as in the Jacobina greenstone belt in the São Francisco craton [136].

6. Discussion

The integration of previous data with new findings presented herein is used to propose a tectono-magmatic evolution of the GAB by reconciling available datasets with isotopic evidence for crust generation. In this section, we provide: (i) interpretations of new U-Pb, Hf-O data (Section 6.1); (ii) a geological evolution for terranes in the GAB (Section 6.2); (iii) a model for crust formation (Section 6.3), and (iv) insights into the relation between crustal architecture and gold systems in the GAB (Section 6.3).

6.1. Hf-O Isotopes through Time

Hafnium and oxygen compositions of igneous zircons from terranes in the southern GAB define a remarkable progression that implies a partially linked crustal evolutionary history. The Hf-O isotope trends define four major groups at (i) 2890–2820 Ma, (ii) ~2060 Ma, (iii) 630–610 Ma, and (iv) 530 Ma. The significance of these groups and the transitions between them are explored below.

Superchondritic to near chondritic Hf isotopic evolution across 2890–2820 Ma TTG terranes reveals at least 70 m.y. of mantle-derived magmatism by extraction of melts from similar mildly depleted reservoir. The compatible Hf isotope arrays of Archean rocks favour the consanguinity of these terranes. Conversely, analogous U-Pb magmatic ages argue for a shared Mesoarchean evolution. Older crust formation events proposed by previous studies [23,25,28] based on Sm-Nd data is contentious for two main reasons. First, Sm-Nd model ages are only applicable to estimate the timing of crust differentiation represented by single crustal extraction [137], which disagrees with dominantly negative εNd values obtained for these rocks [28]. Second, alteration of accessory minerals controlling the Nd content (e.g., monazite, allanite, apatite) can cause isotopic re-equilibrium [138,139] and

disturbance of the Sm-Nd systematics is expected given the poly-metamorphic history of the GAB (e.g., [140]). Accordingly, heterogeneous Hf isotope composition and discordance on concordia diagrams of the Caiçara orthogneiss may reflect zircon overgrowths formed during younger metamorphic episodes (e.g., [140,141]).

Another finding that emerges from the Hf isotope dataset is the lack of evidence for collision pinpointed by the isotopic signature of Archean TTG intrusions. The crustal thickening and progressive reworking of older components promoted during collision are manifested by unradiogenic Hf signatures [40,142,143]. Nonetheless, isotopic and geochemical signatures for the Paus de Choro granite fall along with the trend defined by magmatic zircons of the Uvá orthogneiss, which suggests the former sampled material from the source of the latter. Accordingly, the Paus de Choro granite is developed on the margin of the Uvá terrane rather than as an exotic terrane. Additionally, considering the stratigraphic integrity between the Faina and Goiás greenstone belts that separate the Uvá and Caiçara TTG terranes, the Paus de Choro granite is presumably linked to the Uvá terrane.

Oxygen isotopic compositions of 2890–2820 Ma intrusions overall agree with values obtained for Archean igneous zircons worldwide (5.0‰ < δ18O < 7.4‰; [49]), which are interpreted as typical of magmas in equilibrium with the mantle. Low δ18O values related to high U-Pb discordance and Th/U ratios largely from the Caiçara orthogneiss suggest some degree of isotopic disturbance (Supplementary Figure S8). Radiogenic lead loss due to isotopic disturbance can be promoted by hydrothermal alteration and/or metamorphism [37,144,145].

The shift to unradiogenic Hf values recorded by 2061 Ma Pink Syenite indicates the prevalence of crustal reworking from initially more radiogenic Archean values and suggests continental collision (e.g., [40,142]). Similarly, early collision and minor reworking is suggested by the unradiogenic signature of ~ 2880 Ma inherited zircons in the Pink Syenite. The low δ18O values of inherited grains (~4‰) can reflect high-temperature alteration of the source to the magmas from which these zircons crystallized. High oxygen ratios (~6–7‰) of Pink Syenite igneous grains imply a minor supracrustal contribution.

The broad range of unradiogenic Hf signatures (−3.0 to −10.5) encapsulated by 630–610 Ma K-rich magmatism supports melting of an old crust for their formation. This agrees with negative εNd (−5.1 to −5.7) and Mesoproterozoic model ages (~1440 Ma) registered for Itapuranga granites [146], and with mixed εNd (−4.2 to +2.1) and Mesoproterozoic model ages (~1100 Ma) obtained for the Rio Caiapó granite [147]. All zircons with δ18O > 8.0‰ are confined to the 630–610 Ma age group. High δ18O ratios are diagnostic for the contribution of a component (likely sedimentary) formed by low-temperature processes (e.g., [50]). Thus, anatexis of metasedimentary crust is inferred from the elevated oxygen composition of this group. Tectonic transport of sedimentary material into depth during synchronous granite generation is reported in other collisional events along convergent margins, e.g., Lachlan and Ross-Delamerian orogens [40].

Strongly unradiogenic εHf and mantle-like δ18O values of the 530 Ma Serra Negra granite suggest the predominance of crustal reworking following a linear decrease from initial mostly near-chondritic Archean signatures. Derivation from an older sialic crust is reinforced by negative εNd (−3.0 to −4.0), 1100–1900 Ma TDM model ages [147,148], and ~2680 Ma inheritance [149]. Accordingly, similar chemistry and isotopic signatures with the Uvá orthogneiss evoke shared sources and/or similar mechanisms forming the Serra Negra granite (Supplementary Figure S9). A regression line linking εHf isotope compositions of these samples highlights identical isotopic evolution from an Archean protolith (Supplementary Figure S6). The linear decrease from ~2870 Ma mostly near chondritic signatures implies successively younger magmas likely exploited the same structural conduits as older batches. This scenario challenges the heterogeneity attributed to disparate sources and growth paths across terranes of the GAB [11,12,71].

6.2. Geological Evolution of the GAB

The tectono-magmatic history of the GAB is expressed by three main events in the Archean, Paleoproterozoic, and Neoproterozoic (Figure 6A).

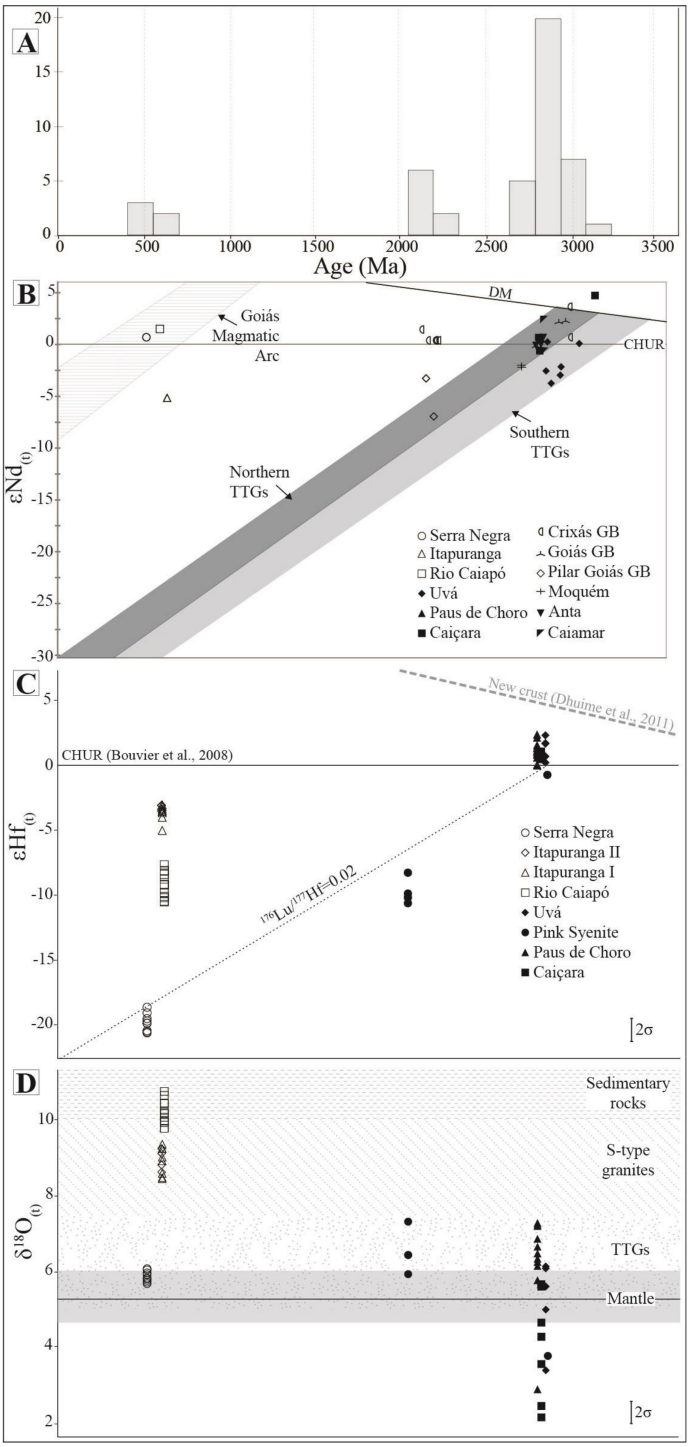

Figure 6. (**A**) Histogram of crystallization ages for igneous rocks in the GAB; (**B**) previously published εNd(T) data for supracrustal rocks and felsic magmatic rocks in the GAB [21,23,25,26,75,77,87,147,150–152]; (**C**) zircon εHf(T) isotope data for the southern GAB (error bar indicated at 2σ), and (**D**) zircon $\delta^{18}O$ isotope composition for granitic intrusions in the southern GAB (error bar indicated at 2σ).

Amphibolite faces metamorphism in the Archean is recorded by 2772 ± 6 Ma U-Pb zircon age and 2711 ± 34 Ma titanite U-Pb age for the Crixás-Açu gneiss in the Caiamar terrane [21,22], whereas in the southern GAB metamorphism is dated at ca. 2840 Ma [25]. This suggests that the stabilization of the GAB occurred at ca. 2700 Ma.

Two main tectonic events are recorded in the GAB during the Paleoproterozoic [22]. An early crustal extension manifested by ~2300 Ma epicratonic mafic dike swarm in TTG terranes [85,94] and a compressional deformation revealed by ~2150 Ma metamorphic titanite [72]. Contrary to the age range reported for lower stratigraphic sequences of the Crixás, Faina, and Goiás greenstone belts at ca.3000–2800 Ma, volcanism at Guarinos and Pilar de Goiás greenstone belts dates approximately 2200 Ma [11,75,76]. Yet, sedimentary rocks of all greenstone belt sequences were deposited in the Paleoproterozoic [11]. Episodic magmatism during the Paleoproterozoic is represented by: (i) 2146 Ma Posselândia diorite stock hosted in NW-trending shear zone that crosscuts the Hidrolina TTG [109], (ii) 2145 Ma albite granite emplaced within N-verging thrust faults intrusive in metasedimentary rocks of the northern greenstone belts [72], (iii) Pink Syenite intrusion coeval with Au-related deformation event in the Faina greenstone belt, and (iv) 2170 Ma mafic dikes that crosscut Au-mineralized orebodies at the Crixás greenstone belt [74].

Tectonic quiescence lasted until the Neoproterozoic when the GAB was amalgamated to the Brasília fold belt. The influence of a Neoproterozoic tectonic event is reflected by thermal disturbance recorded in granite-gneisses of the GAB. Evidence include a zircon U-Pb SHRIMP 625 Ma age interpreted to result from the anatexis of the Caiçara terrane [28] and zircon U-Pb LA-ICP-MS 729 Ma age for leucogranite intrusive in the Guarinos greenstone belt [10]. However, the interpretation of these data is contested. First, thermal disturbance of isotopic systems in polydeformed terranes does not necessarily denote an intrusive event (e.g., [28]). Secondly, the shortage of analyses, method applied and lack of synchronous magmatism brings into question the reliability of the data reported for leucogranite in the Guarinos greenstone belt. Thus, more research needs to be conducted to address these interpretations.

In the northern GAB (Figure 7), TTG magmatism occurred in two main stages spanning 70 m.y. [22]. Early stage 2845–2785 Ma tonalite to granodiorite (with minor granite) orthogneisses show juvenile εNd signatures (e.g., Anta and Caiamar terranes). Inherited zircon xenocrysts in early stage intrusions suggest the contribution of an older sialic crust of up to 3300 Ma, which does not outcrop [22]. The subsequent magmatic stage forms 2711 to 2707 Ma granodiorite to granite orthogneisses with crustal εNd signature (e.g., Moquém terrane). The isotopic zonation reflected by the εNd signature of TTG terranes in the northern GAB is interpreted to denote an eastward migration of crustal growth [22]. The diachronous evolution of TTG granite-gneiss terranes in the northern GAB is augmented by whole-rock geochemistry for these rocks [19]. According to the latter, pre- to syn-collisional early stage intrusions show sub-alkaline to calc-alkaline affinities, whereas syn-collisional to post-tectonic late-stage intrusions are calc-alkaline to metaluminous.

The Caiamar terrane includes the ~2840 Ma Águas Claras and Tocambira intrusions, which are intruded by the magmatic protoliths of the 2820 Ma Crixás-Açu gneiss [22]. The Hidrolina terrane is formed by 2785 Ma granodiorite that is intruded by 2146 Ma Posselândia diorite [22,109]. The Anta terrane includes 2840–2820 Ma granodiorite orthogneisses intruded by the 2790 Ma Chapada granite [22,23,151]. Fractionated REE, particularly HREE, and slightly positive εNd (0.7) recorded by the Anta orthogneisses support the contribution of an older crust in its genesis [23].

In the southern GAB (Figure 8), two major pulses of magmatism spanning 40 m.y. in the Uvá and Caiçara terranes are recorded by mostly juvenile 3040–2930 Ma and slightly crustal-derived 2890–2820 Ma orthogneisses, e.g., Paus de Choro granite [23–25,77,147] and this study. Zircon age inheritance at 3090–3050 Ma suggests the involvement of up to 3100 Ma crust. Older model ages of up to 3500 Ma obtained in previous studies [147] from samples with high $^{147}Sm/^{144}Nd$ ratios may reflect fractionation of the Sm-Nd system during metamorphism [28].

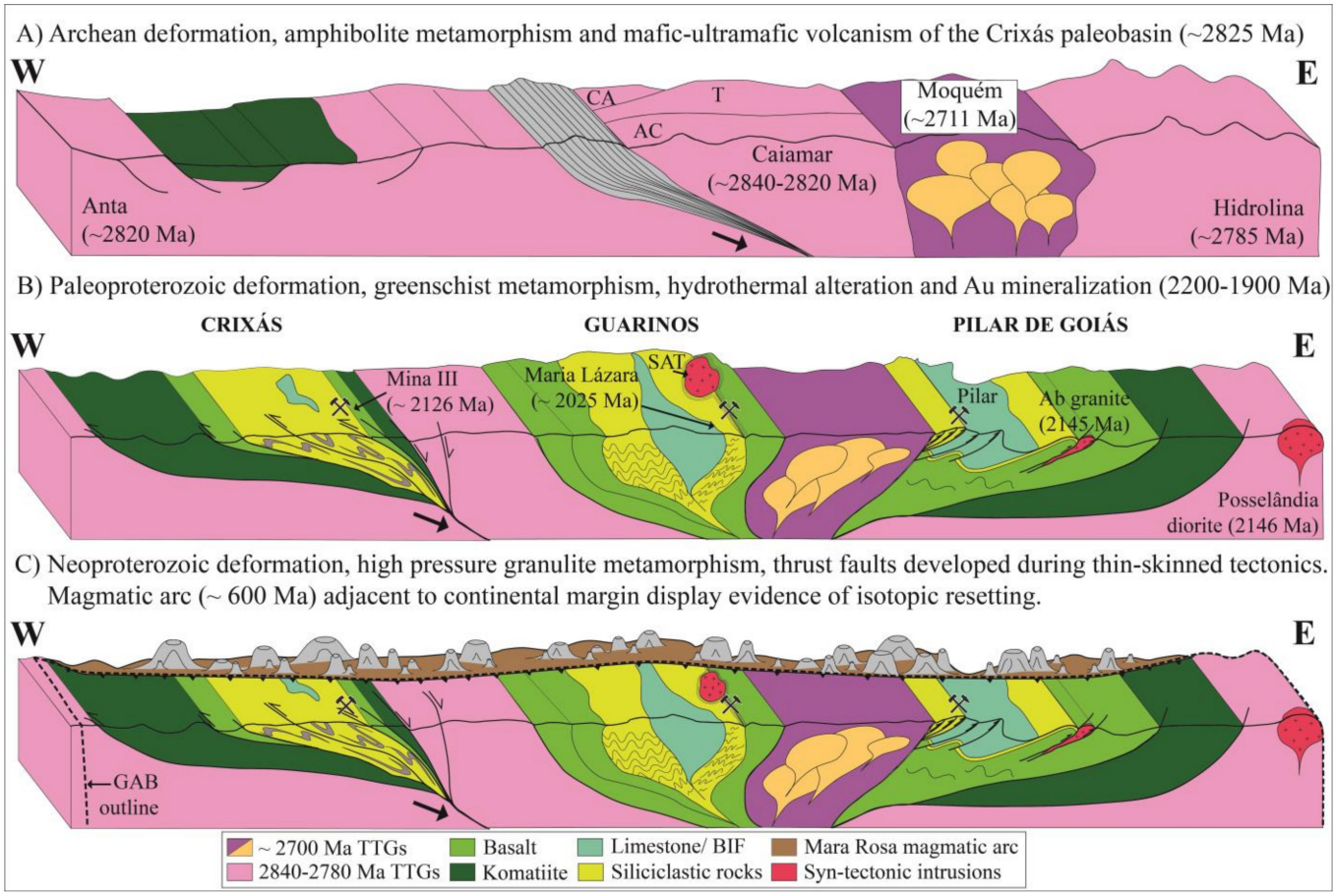

Figure 7. Schematic block diagrams showing the evolution of the northern GAB during (**A**) Archean event, (**B**) Paleoproterozoic event, and (**C**) Neoproterozoic event (not to scale). Abbreviations in A for the Caiamar TTG terrane refer to Crixás-Açu (CA), Tocambira (T), and Águas Claras (AC).

In the northern GAB, volcanic sequences of the Crixás greenstone belt reveal spinifex textures [92,136] typically associated with komatiite flows [150]. Ultramafic flows are overall characterized by smoothly sloping, LREE-rich patterns, whereas basalts show flat REE patterns and slight depletion in both LREE and HREE [150]. The metabasalts of the Guarinos greenstone belt have a tholeiitic affinity, slightly fractionated REE patterns and negligible negative Eu anomaly consistent with a back-arc environment [153]. Volcanic rocks in the Pilar de Goiás greenstone belt show flat to slightly fractionated REE patterns compatible with the ones from tholeiitic lavas [96].

In the southern GAB, preserved pillowed structures in lower volcanic sequences attest to the subaqueous nature of these sequences that allowed their correlation with komatiites [77]. According to the former authors, the geochemistry of lower ultramafic rocks is characterized by tholeiitic, sub-alkaline to calc-alkaline affinities and flat REE patterns. Mafic sequences of both greenstone belts are LREE-rich, HREE-poor and show subtle negative to positive Eu anomalies [77].

6.3. Archean Crust Formation: Towards a Model

The GAB records zircon U-Pb crystallization ages and zircon inheritance peaks at 3000, 2800 and 2700 Ma (Figure 6A). Magmatic quiescence occurs between 2930–2890 Ma (in the south) and 2840–2710 Ma (in the north). Temporal and spatial relationships between TTG plutonism and greenstone belt development require a tectonic process that allows the coeval formation of both komatiite-tholeiite basalt sequences and calc-alkaline magmatism.

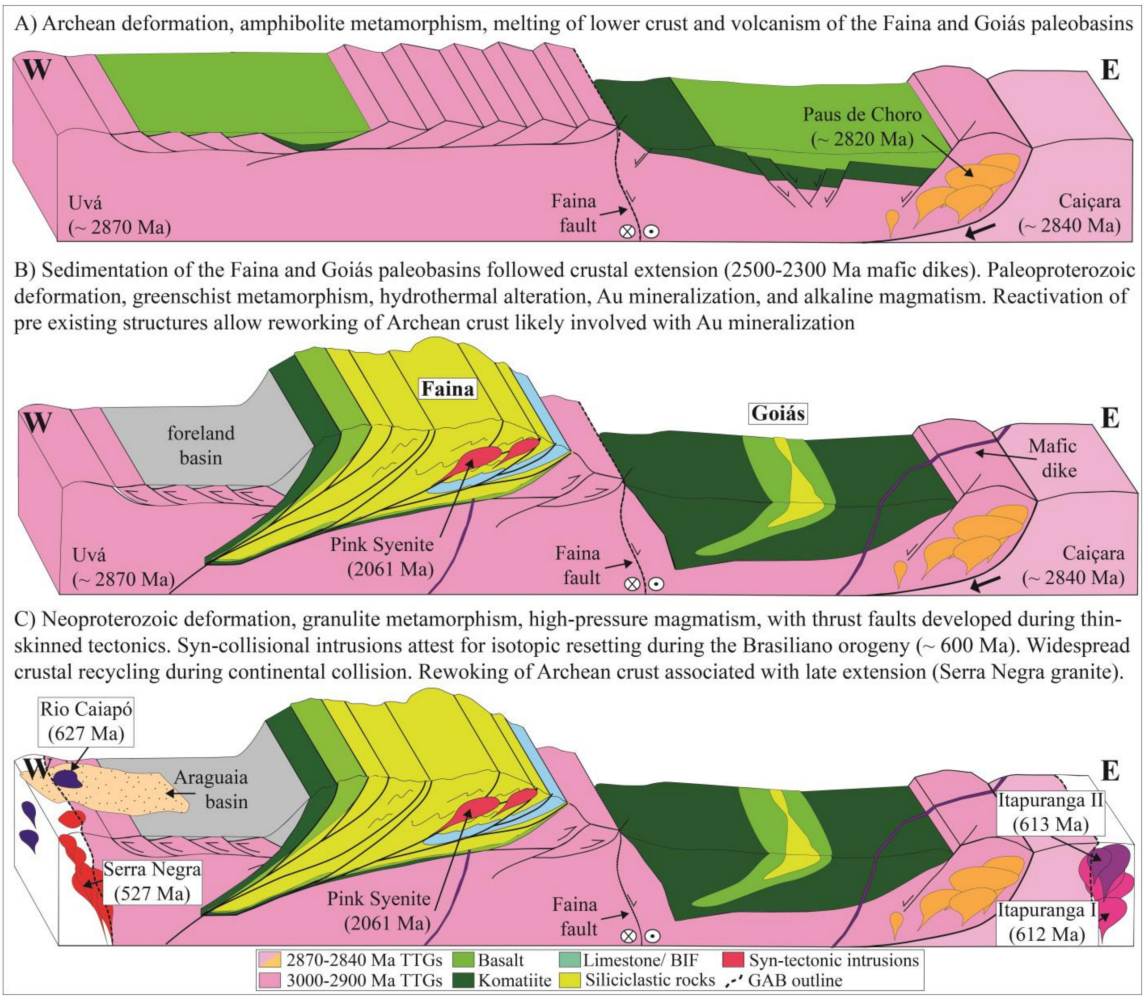

Figure 8. Schematic block diagrams showing the evolution of southern GAB during (**A**) Archean event, (**B**) Paleoproterozoic event, and (**C**) Neoproterozoic event (not to scale).

The geodynamics of Archean crustal growth has been debated for decades (e.g., [154–157]). Archean cratons are dominated by 'arc-like' tonalite-trondhjemite-granite, i.e., TTG association [158,159] and 'plume-like' komatiite-tholeiite basalt association [160,161]. As a result, Archean crustal growth models reflect a dichotomy between subduction and plume-related processes, and disagreements persist over the timing of onset of plate tectonics [162–167].

Typical upward younging, tholeiitic basalt-komatiite association and geochemistry similar to Archean greenstone belts make oceanic plateau settings an appealing premise [168–170]. In this context, the production of contemporaneous tholeiitic basalt-komatiite and TTG-like magmas is assumed to occur by infracrustal melting at the base of a thick plateau [171]. Therefore, oceanic plateau [172,173], sagduction [174], plume-derived continental drift [175], and plume-arc [160] are often offered to explain the generation of granite-greenstone terranes by plume-driven processes [176].

An argument against plume-driven models is that basalts derived from plumes are commonly associated with low water contents and, therefore, are an unlikely source for voluminous partial melt [177]. The melting of an anhydrous source contrasts with the ubiquitous hydrous mineralogy associated with that of Archean TTGs [178]. Apart from that, the refractory and cumulus nature typical of lower mafic-ultramafic sequences is likely an infertile source for evolved magmas [177]. Yet, investigations have shown that some plume-derived basalts provide an appropriate geochemical [179] and isotopic [180] source for Archean TTGs.

Recent interpretations propose a sagduction, plume-related scenario for the early evolution of terranes in the GAB [181]. Several studies advocate for similar models to explain Archean geodynamics [164,182–185]. According to this paradigm, granitic rocks are formed via partial melting of a thick basaltic pile in an oceanic plateau [164], which implies mantle plume magmatism. However, this hypothesis is challenged by several arguments. Based on Jost et al. [181], after the formation of ≤3300 Ma sialic crust (presently not exposed in the GAB), rifts induced by a hotspot or mantle plume led to the production of ca. 3000 Ma komatiite and pillowed basalts in an oceanic island, stratovolcano, or plateau environment. According to the same authors, diapiric emplacement of felsic magmatism attributed to the Anta and Caiamar terranes took place at least 200 m.y. after crystallization of their igneous protoliths. However, crust formation in an oceanic plateau would result in upward younging and low metamorphic grade that preclude tectonic stacking via horizontal tectonics [186]. This disagrees with high-temperature, amphibolite faces metamorphism, and stacking of the stratigraphy recorded in Archean rocks of the GAB (e.g., [11,12,72]).

The Nd isotopic record for the Anta (0.0 to 0.7; [22,23]) and Caiamar terranes (−0.6 to 2.4; [22]) implies dominantly juvenile sources. Plume-related generation of TTG in an oceanic plateau could be either by: (i) density inversion [164], (ii) melting of previous crust [155], or (iii) differentiation of underplated coeval basaltic melts. The two first options imply reworking of older sources, which conflicts with the isotopic record of these terranes. In turn, the last option would reflect higher εNd values that are also inconsistent with the juvenile signature presented by previous studies [22,23].

This is supported by the in-situ U-Pb and Hf-O dataset provided for granitic rocks in the southern GAB. Near-chondritic εHf values of 2870–2840 Ma magmatic zircons of the Caiçara and Uvá orthogneisses are consistent with a major mantle-derived input. The higher εHf values for the 2820 Ma Paus de Choro granite suggest generation by melting of juvenile crust recently formed from depleted mantle (e.g., [141]), which indicates decreasing crustal reworking over time. In contrast, unradiogenic εHf values of >2880 Ma Pink Syenite inherited zircons suggest reworking of an older crust, but the limited dataset gives no insight into the nature of that crust.

Another point of contention involving plume-related models is whether the triangular, narrow, cusp-shaped, and kilometre-deep keel shape of the Crixás greenstone belt [187] can be used to support a plume-related model invoked for the Archean generation of continental crust in the GAB, as proposed by Jost et al. [181]. Besides the extremely limited evidence provided for vertical tectonics, the parameters used to demonstrate this hypothesis are vague. For example, there is no conspicuous record of steep regional structures in the Crixás greenstone belt. This can be partially explained by the intense deformation and low preservation of any earlier formed structures in the area. Yet, low-pressure, contact-style metamorphism characterized by isograds concentrically distributed around TTG domes varying from high-temperature (i.e., amphibolite facies) adjacent to the intrusions to low-temperature (i.e., prehnite-pumpellyite facies) away from the intrusions (e.g., [188]) is also not consistent with previous structural-metamorphic investigations conducted in the Crixás greenstone belt [11,12,18,102,125].

An additional piece of evidence against a plume-related hypothesis is that, despite being proposed to explain the formation of other granite-greenstone associations, e.g., in the Kaapvaal Craton in South Africa and the Pilbara Craton in Western Australia [189], the extremely thick mafic-ultramafic sequence characteristic of these areas (the order of several kilometres) is much more pronounced than the volcanism associated with terranes in the GAB (up to 900 m in the Pilar de Goiás greenstone belt) [11,18,71]. However, the genesis of basal supracrustal sequences in the GAB is still poorly explored and a plume-related origin is not completely disregarded. Hybrid examples of the two end-members of models proposed for Archean crust formation are reported in other cratons (e.g., [190–192]). Therefore, further investigation is required to define the precise genesis of Archean crust in the GAB.

In terms of geochemistry, volcanic rocks in greenstone belts are generally characterized by: (i) plume-related tholeiitic basalt-komatiite in oceanic and continental plateau [168,193], and (ii) subduction-related calc-alkaline basalts, andesites, dacites and rhyolites with other minor rock types, e.g., boninites, adakites, and Nb-rich basalts [194–197]. The derivation of tholeiitic basalt-komatiite associations in greenstone belts has been attributed to high-temperature plume activity [189,193]. Alternatively, the subduction-related origin of this association in fore-arc settings have been proposed based on Phanerozoic boninites (e.g., Barberton greenstone belt) [198]. Boninites, formed by hydrous melting of the refractory mantle at shallow depths [199], are intrinsically related to early subduction in intra-oceanic fore-arc settings [200].

Analogous chemical composition of komatiites with modern boninites (SiO_2 > 53%, Mg# > 60, TiO_2 < 0.5 wt. %) [199] supports a subduction-related origin of komatiites in the southern GAB [77]. The flat REE patterns and Nb-rich contents of mafic sequences, typical of back-arc and Nb-rich basalts, reinforce the involvement of subduction processes for the genesis of volcanic rocks in these sequences [77]. Therefore, volcanism in the southern GAB is interpreted to result from fore- to back-arc rifts during accretionary extension, whereas calc-alkaline intrusions are proposed to form at transient compression by shallow subduction in the southern GAB.

In the northern GAB, a whole-rock Sm-Nd isochron age of 2825 ± 98 Ma and near zero εNd (0.6) values reported for komatiite flows in the Crixás greenstone belt [150] attest to their juvenile source. Other studies propose a depleted mantle source formed in an oceanic crust based on whole-rock Sm-Nd isochron at 2998 ± 70 Ma and εNd(T) of 2.4 for lower metavolcanic rocks of the Crixás greenstone belt [87]. Nd isotopic signature and U-Pb detrital zircon geochronology suggest juvenile sources with minor contributions of reworked crust for metasedimentary rocks of the Crixás greenstone belt [87,101]. This data agrees with the above arguments for subduction rather than a plume-related origin of these rocks. In the southern GAB, the 2061 Ma Pink Syenite intrusion is compatible with the onset and prevalence of reworking. The dashed line in Figure 6C shows the Hf isotope evolution of 2870 Ma crust (Uvá TTG) towards strongly negative zircon εHf(t) values represented by the Serra Negra granite. The trend from a 2870 Ma primitive mantle has a slope that corresponds to a $^{176}Lu/^{177}Hf$ value of 0.02, which agrees with that of a mafic crust.

Compression in Phanerozoic orogens is expressed by decreasing magmatism, isotopic flare-ups, and distinct bulk rock geochemistry (e.g., [40,143]). The transition to unradiogenic Nd/Hf isotopes in accretionary margins at this time is related to increased contamination of magmas in the upper plate. In the northern GAB, the increasingly unradiogenic Nd signature from the western to the eastern TTG terranes (Figure 6B) favours compression. Thus, calc-alkaline intrusions are proposed to form by episodic compression during shallow subduction and eastward migration of the arc in the northern GAB (e.g., [22,201]). This is compatible with geochemical results on TTG terranes from Vargas [19]. Moreover, diagnostic geochemical and geological parameters provided by Kerr [202] for volcanic sequences from distinct tectonic settings support the arc-like signature of lower mafic-ultramafic rocks in the northern GAB greenstone belts (e.g., [153]). Nevertheless, limited Nd isotopic signature available for the supracrustal rocks, especially for Guarinos and Pilar de Goiás, hampers more detailed correlations.

6.4. Linking Crustal Architecture to Gold Mineralization

Crust generation and destruction by subduction-collision in convergent margins has shaped the continental crust throughout Earth's history [203]. The evolution of continental crust promotes a diverse lithospheric architecture that effectively controls the development of preferential pathways for magmas and fluids [7]. Crustal architecture plays a major role in the location of lithospheric-crustal scale structures controlling large orogenic Au-related hydrothermal systems [8]. The potential for mineralization in cratonic blocks worldwide is illustrated by the occurrence of gold [13,204–206], base metals [207–210], and iron [211–214].

As recognized by previous studies, the addition of juvenile material into the crust enhances the gold fertility in the terrane [215–217]. Studies in the Yilgarn craton suggest the input of juvenile crust (εNd > 0) before and after gold mineralization acted as a potential source of this metal [29]. A similar U-Pb-O-Hf isotope approach was applied in this study to provide insights into potential links between crust-mantle evolution and the development of gold systems in the GAB (Figure 9).

The geochemistry of TTGs from the GAB indicates their formation in volcanic arcs associated with subduction zones ([19,22,77], this work). The hypothesis that a >3200 Ma older crust may have existed, based on U-Pb and Sm-Nd T_{DM} model ages [22,25,77], is considered equivocal for two reasons. First, the reworking of these rocks indicated by geochronology and isotopic geochemistry is more likely while the magmas are still hot rather than ~300 Ma years after their emplacement. In addition, a lack of exposed crust or inherited U-Pb ages older than 3100 Ma argues against the presence of continental crust before this time. The inherent uncertainties of Nd model ages are well known [137], and the zircon Hf isotope data show little evidence for reworking of substantially older crust (Figure 6C). A more plausible explanation for the extraction of these primitive melts involves crustal reworking occurring shortly after emplacement of the original Archean crust.

In the northern GAB, two major magmatic events are represented by ~2770 Ma rocks with juvenile-like εNd, and ~2700 Ma rocks with εNd values indicative of crustal contribution for the formation of these magmas. The new zircon in situ U-Pb-O-Hf results (Figure 6) indicate that the crustal formation in the southern GAB likely involved the negligible reworking of an older crust of approximately 2870 Ma, which overlaps with an older magmatic event proposed by Queiroz et al. [22] for the northern GAB. This is consistent with previous interpretation by Jost et al. [25]. In turn, Archean geodynamics for the southern GAB can be defined by the following sequence as: (i) 2960–2920 Ma fore-arc/back-arc assembly with positive εNd (+2.2 to +2.8) indicative of a juvenile arc, followed by (ii) ca. 2800 Ma continental arc with slightly negative εNd (−0.1) that indicates minor crustal contribution during genesis of tonalite magmatism [77].

Gold deposits in the GAB are spatially located in the greenstone belts [12], especially along major structures adjacent to their boundaries with the TTGs and at intersections of multiple regional structures (e.g., [8,218]). The metasedimentary and metavolcanic host rocks of gold deposits are mostly characterized by unradiogenic εNd [87] indicative of an old, reworked source. In the southern GAB, the emplacement of syn- to late-orogenic Pink Syenite with unradiogenic εHf signature coupled with mantle-like $\delta^{18}O$ values indicates a link between mantle, crust, and gold-related deformation. Similar geochemistry, geochronology, and isotopic signatures with younger intrusions, e.g., the Serra Negra granite, and the correlation of the latter with newly discovered Cu-Au deposits in the region (e.g., Fazenda Nova; [149]) have implications for regional exploration, and they support the importance of juvenile contribution for the generation of gold deposits in the GAB.

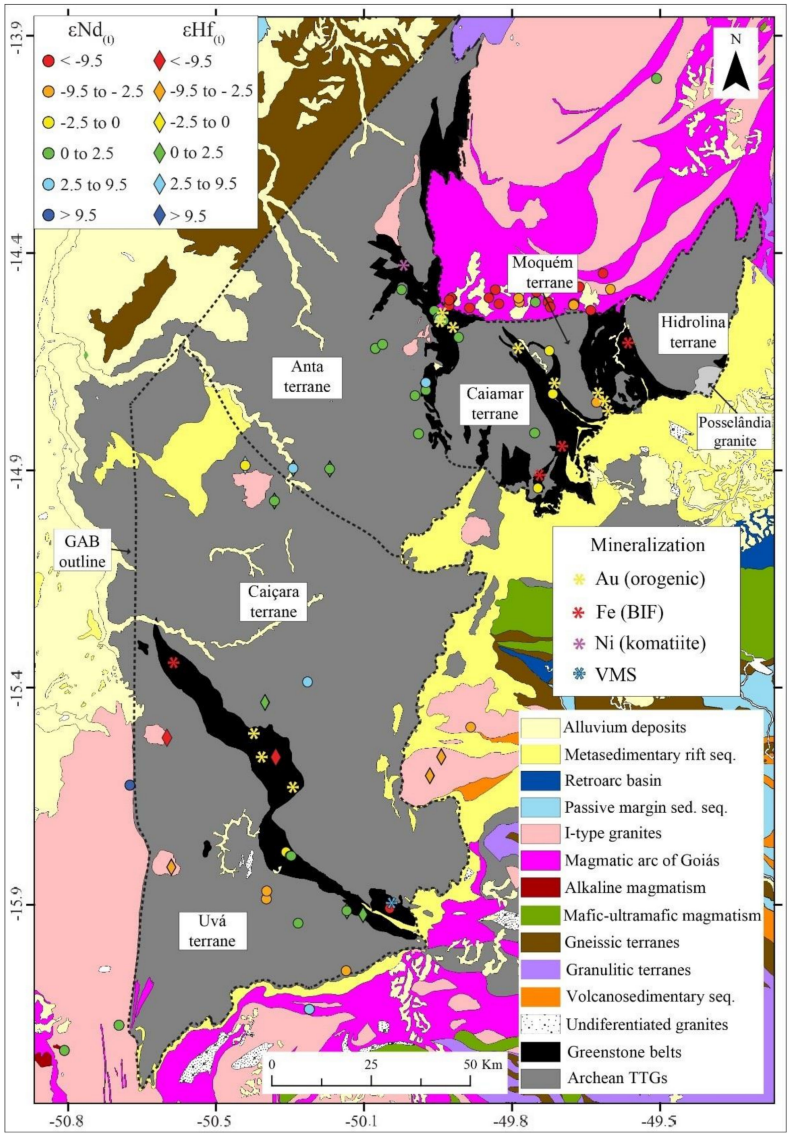

Figure 9. Map showing available εNd and zircon εHf dataset in the Goiás Archean Block. The diachronous stabilization of TTGs is evidenced by crustal growth migration towards the east in the northern GAB, suggested by increasingly crustal input eastward, whereas dominant juvenile TTG crust in the south. References for isotopic data: [22–25,28,75,147,152] and this work.

7. Conclusions

The GAB is the only Archean crust in central Brazil and a significant host of important gold systems. Gold mineralization in the GAB is characterized by structurally controlled orebodies, similar white mica-quartz-pyrite ± chalcopyrite hydrothermal assemblages, as well as comparable temperature and pressure conditions of ore formation. Orebodies are mainly controlled by subtly W- to NW-dipping foliation, axial planar to subhorizontal NW-striking isoclinal folds, and gently S-dipping thrust faults. Typical host rocks include carbonaceous schist, metabasalt, quartzite, and marble. Gold-related hydrothermal alteration minerals overprint greenschist to upper amphibolite faces metamorphic assemblages, therefore, are considered to represent post-peak metamorphism.

The regional isotopic signatures of igneous and sedimentary rocks offer new insights into the genesis of gold systems and the crustal evolution of the GAB. This is promoted by a combination of geological datasets at different scales, such as geochemistry and geochronology, and emphasis on gold-related ore-forming processes. The large-scale geodynamic context presented aims to boost mineral exploration strategies in the GAB.

Available geochemistry combined with isotope-time trends are used to reconcile models for the generation of Archean crust. Similar isotopic signatures highlight the secular homogeneity across the granite-greenstone terranes of the GAB that imply these terranes shared similar magma sources, tectonic processes and/or deep-seated structures during their formation.

Gold and other minor mineral deposits (e.g., Ni deposit in the Crixás greenstone belt) tend to concentrate at the borders between greenstone belts with TTG terranes, and adjacent to tectonic boundaries. The formation and distribution of mineral deposits in greenstone belts is predicted by back-arc settings, which can supply the metal budget essential for the development of gold systems and other mineralization in the GAB, such as VMS deposits.

Supplementary Materials: The following are available online at https://www.mdpi.com/article/10.3390/min11090944/s1. Table S1: Geochemical data of granitic rocks of the southern GAB; Table S2: Geochronology and Isotopic dataset of granitic rocks of the southern GAB; Table S3: Results of SHRIMP U-Pb zircon geochronology; Table S4: Results of SHRIMP U-Pb analyses of Archean (-Paleoproterozoic) sample; Table S5: Mean weighted analyses of standard materials used for U-Pb dating; Table S6: Results of Lu-Hf analyses of granitic samples in the southern GAB; Table S7: Results of standard materials used to calibrate in- situ Lu-Hf analyses; Table S8: Results of oxygen isotopic analyses of granitic rocks in the southern GAB; Table S9: Results of standard materials used to calibrate in-situ oxygen analyses; Figure S1: Geological map of southern GAB with the location of analysed samples; Figure S2: Hand sample and cross-polarized photomicrograph; Figure S3: Hand sample and photomicrograph; Figure S4: Cathodoluminescence (CL) images of representative zircon grains from the southern GAM; Figure S5: Concordia diagrams for studied granitic rocks of the southern GAB; Figure S6: εHf vs crystallization and inheritance ages of intrusions; Figure S7: δ18O vs emplacement age of granitic rocks in the southern GAB.

Author Contributions: Conceptualization, J.B. and A.I.S.K.; methodology, J.B. and A.I.S.K.; software, J.B. and A.I.S.K.; validation, J.B., A.I.S.K. and S.G.H.; formal analysis, J.B.; investigation, J.B. and A.I.S.K.; resources, J.B.; data curation, J.B., A.I.S.K. and S.G.H.; writing—original draft preparation, J.B.; writing—review and editing, J.B., A.I.S.K. and S.G.H.; visualization, J.B.; supervision, A.I.S.K. and S.G.H.; project administration, J.B.; funding acquisition, J.B. All authors have read and agreed to the published version of the manuscript.

Funding: The research was funded by CNPq ("Conselho Nacional de Desenvolvimento Científico e Tecnológico"; Project No. 207220/2014-0). Instrumentation for Hf isotope analysis at UWA was funded in part by the Australian Research Council (LE100100203 and 150100013).

Data Availability Statement: Not applicable.

Acknowledgments: We thank the volume guest editors Lydia Lobato and Rosaline Silva for the invitation and opportunity to contribute to this Special Issue. This work is a result of a PhD project completed by Jessica Bogossian at the CET-UWA (Centre for Exploration Targeting, School of Earth Sciences, University of Western Australia). To Tyler Baril for the kind support and valuable insights.

Conflicts of Interest: The authors declare no conflict of interest.

References

1. Goldfarb, R.J.; Groves, D.I.; Gardoll, S. Orogenic gold and geologic time; a global synthesis. *Ore Geol. Rev.* **2001**, *18*, 1–75. [CrossRef]
2. Bierlein, F.P.; Groves, D.I.; Goldfarb, R.J.; Dube, B. Lithospheric controls on the formation of giant orogenic gold deposits. *Minim. Depos.* **2006**, *40*, 874–886. [CrossRef]
3. Bierlein, F.P.; Groves, D.I.; Cawood, P.A. Metallogeny of accretionary orogens—The connection between lithospheric processes and metal endowment. *Ore Geol. Rev.* **2009**, *36*, 282–292. [CrossRef]
4. Groves, D.I.; Condie, K.C.; Goldfarb, R.J.; Hronsky, J.M.A.; Vielreicher, R.M. Secular changes in global tectonic processes and their influence on the temporal distribution of gold-bearing mineral deposits. *Econ. Geol.* **2005**, *100*, 203–224. [CrossRef]
5. Goldfarb, R.J.; Groves, D.I. Orogenic gold: Common or evolving fluid and metal sources through time. *Lithos* **2015**, *233*, 2–26. [CrossRef]
6. Ketchum, J.W.F.; Ayer, J.A.; van Breemen, O.; Pearson, N.J.; Becker, J.K. Pericontinental Crustal growth of the Southwestern Abitibi Subprovince, Canada—UPb, Hf, and Nd Isotope evidence. *Econ. Geol.* **2008**, *103*, 1151–1184. [CrossRef]

7. Begg, G.C.; Griffin, W.L.; Natapov, L.M.; O'Reilly, S.Y.; Grand, S.; O'Neill, C.J.; Poudjom Djomani, Y.; Deen, T.; Bowden, P. The lithospheric architecture of Africa: Seismic tomography, mantle petrology and tectonic evolution. *Geosphere* **2009**, *5*, 23–50. [CrossRef]
8. Blewett, R.S.; Henson, P.A.; Roy, I.G.; Champion, D.C.; Cassidy, K.F. Scale-integrated architecture of a world-class gold mineral system: The Archaean eastern Yilgarn Craton, Western Australia. *Precis. Res.* **2010**, *183*, 230–250. [CrossRef]
9. Pimentel, M.M.; Fuck, R.A.; Jost, H.; Ferreira Filho, C.F.; Araújo, S.M. The basement of the Brasília Fold Belt and Goiás Magmatic Arc. In Proceedings of the Tectonic Evolution of South America, 31st International Geological Congress, Rio de Janeiro, Brazil, 6–17 August 2000; pp. 195–230.
10. Rodrigues, V.G. Geologia do Depósito Aurífero do Caiamar, Greenstone Belt de Guarinos: Um Raro Depósito Associado a Albitito Sódico. Master's Thesis, University of Brasília, Brasília, Brazil, 2011.
11. Jost, H.; Carvalho, M.J.; Rodrigues, V.G.; Martins, R. Metalogênese dos Greenstone belts de Goiás. In *Metalogênese das Províncias Tectônicas Brasileiras*; Silva, M.G., Neto, M.B.R., Jost, H., Kuyumjian, R.M., Orgs.; CPRM: Belo Horizonte, Brazil, 2014; pp. 141–168.
12. Jost, H.; Fortes, P.T.F.O. Gold deposits an occurrences of the Crixás Goldfield, Central Brazil. *Minim. Depos.* **2001**, *36*, 358–376. [CrossRef]
13. Robert, F.; Poulsen, K.H.; Cassidy, K.F.; Hodgson, C.J. Gold Metallogeny of the Superior and Yilgarn Cratons. In *Economic Geology One Hundredth Anniversary Volume (1905–2005)*; Hedenquist, J.W., Thompson, J.F.H., Goldfarb, R.J., Richards, J.P., Eds.; Society of Economic Geologists: Littleton, CO, USA, 2005.
14. Pulz, G.M. Geologia do Depósito Aurífero Maria Lázara (Guarios, Goiás). Master's Thesis, University of Brasília, Brasília, Brazil, 1990.
15. Jost, H.; Queiroz, C.L. Síntese da evolução crustal do Bloco Arqueano de Goiás. In Proceedings of the 44th Brazilian Congress of Geology, Curitiba, Brazil, 26–31 October 2008; Volume 1, pp. 10–12.
16. Marques, J.C.; Jost, H.; Creaser, R.A.; Frantz, J.C.; Osorio, R.G. Age of arsenopyrite gold-bearing massive lenses of the Mina III and its implications on exploration, Crixás greenstone belt, Goiás, Brazil. In Proceedings of the III Brazilian Symposium of Metallogeny, Gramado, Brazil, 2–5 June 2013. Extended Abstracts.
17. Pimentel, M.M.; Jost, H.; Fuck, R.A. O Embasamento da Faixa Brasília e o Arco Magmático de Goiás. In *Geologia do Continente Sul-Americano: Evolução da Obra de Fernando Flávio Marques de Almeida*; Mantesso-Neto, V., Bartorelli, A., Carneiro, C.D.R., Neves, B.B.B., Org.; Beca Produções Culturais Ltd.a.: São Paulo, Brazil, 2004; pp. 356–368.
18. Jost, H.; Oliveira, A.M. Stratigraphy of the greenstone belts, Crixás region, Goiás, central Brazil. *J. South Am. Earth Sci.* **1991**, *4*, 201–214. [CrossRef]
19. Vargas, M.C. Geologia dos Granito-Gnaisses dos Terrenos Granito-Greenstone da Região de Crixás, Guarinos, Pilar de Goiás e Hidrolina, Goiás. Master's Thesis, University of Brasília, Brasília, Brazil, 1992.
20. Resende, M.G.; Jost, H. Petrogênese de formações ferríferas e metahidrotermalitos da Formação Aimbé, Grupo Guarinos (Arqueano), Goiás. *Braz. J. Geol.* **1995**, *25*, 41–50. [CrossRef]
21. Queiroz, C.L.; McNaughton, N.J.; Fletcher, I.R.; Jost, H.; Barley, M.E. Polymetamorphic history of the Crixás-Açu Gneisses, Central Brazil: SHRIMP U–Pb evidence from titanite and zircon. *Braz. J. Geol.* **2000**, *30*, 40–44.
22. Queiroz, C.L.; Jost, H.; Silva, L.C.; McNaughton, N.J. U-Pb SHRIMP and Sm-Nd geochronology of granite-gneiss complexes and implications for the evolution of the central Brazil Archean Terrain. *J. South Am. Earth Sci.* **2008**, *26*, 100–124. [CrossRef]
23. Beghelli, L.P., Jr. Charnockitos e Ortognaisses da Porção Centro-Oeste do Bloco Arqueano de Goiás: Dados Geoquímicos e Isotópicos. Master's Thesis, University of Brasília, Brasília, Brazil, 2012.
24. Jost, H.; Fuck, R.A.; Dantas, E.L.; Rancan, C.C.; Rezende, D.B.; Santos, E.; Portela, J.F.; Mattos, L.; Chiarini, M.F.N.; Oliveira, R.C.; et al. Geologia e geocronologia do Complexo Uvá, bloco arqueano de Goiás. *Braz. J. Geol.* **2005**, *35*, 559–572. [CrossRef]
25. Jost, H.; Chemale, F., Jr.; Fuck, R.A.; Dussin, I.A. Uvá Complex, the Oldest Orthogneisses of the Archean-Paleoproterozoic Terrane of Central Brazil. *J. South Am. Earth Sci.* **2013**, *47*, 201–212. [CrossRef]
26. Pimentel, M.M.; Fuck, R.A. Geocronologia Rb-Sr da porção sudeste do maciço de Goiás. *Braz. J. Geol.* **1994**, *24*, 104–111.
27. Pimentel, M.M.; Fuck, R.A.; Alvarenga, C.J.S. Post-Brasiliano (Pan-African) high-K granitic magmatism in central Brazil: Late Precambrian/early Paleozoic extension. *Precis. Res.* **1996**, *80*, 217–238. [CrossRef]
28. Pimentel, M.M.; Jost, H.; Fuck, R.A.; Armstrong, R.A.; Dantas, E.L.; Potrel, A. Neoproterozoic anatexis of 2.9 Ga old granitoids in the Goiás-Crixás block, Central Brazil: Evidence from new SHRIMP U-Pb data and Sm-Nd isotopes. *Geol. USP Série Científica* **2003**, *3*, 1–12. [CrossRef]
29. Mole, D.R.; Fiorentini, M.L.; Cassidy, K.F.; Kirkland, C.L.; Thebaud, N.; McCuaig, T.C.; Doublier, M.P.; Duuring, P.; Romano, S.S.; Maas, R.; et al. Crustal evolution, intra-cratonic architecture and the metallogeny of an Archaean craton. In *Ore Deposits in an Evolving Earth*; Jenkin, G.R.T., Lusty, P.A.J., McDonald, I., Smith, M.P., Boyce, A.J., Wilkinson, J.J., Eds.; Geological Society, Special Publication: London, UK, 2015; Volume 393, pp. 23–80.
30. Morris, P.A. *Composition of the Bunbury Basalt (BB1) and Kerba Monzogranite (KG1) Geo-Chemical Reference Materials, and Assessing the Contamination Effects of Mill Heads*; Geological Survey of Western Australia: Perth, Australia, 2007; Record 2007/14.
31. Stern, R.A. *A New Isotopic and Trace-Element Standard for the Ion Microprobe: Preliminary Thermal Ionization Mass Spectrometry (TIMS) U-Pb and Electron-Microprobe Data. Radiogenic Age and Isotopic Studies: Report 14, 2001*; Geological Survey of Canada: Ottawa, ON, Canada, 2001; p. 11.

32. Stern, R.A.; Bodorkos, S.; Kamo, S.L.; Hickman, A.H.; Corfu, F. Measurement of SIMS Instrumental Mass Fractionation of Pb Isotopes during Zircon Dating. *Geostand. Geoanalytical Res.* **2009**, *33*, 145–168. [CrossRef]
33. Compston, W.; Williams, I.S.; Kirschvink, J.L.; Zichao, Z.; Guogan, M. Zircon ages for the Early Cambrian timescale. *J. Geol. Soc.* **1992**, *149*, 171–184. [CrossRef]
34. Ludwig, K.R. *Squid 1.02, a User's Manual*; Berkeley Geochronological Center Special Publication 2; Berkeley Geochronological Center: Berkeley, CA, USA, 2002; p. 21.
35. Ludwig, K.R. *User's Manual for Isoplot 3, a Geochronological Toolkit for Microsoft Excel*; Berkeley Geochronology Center Special Publication 4: Berkeley, CA, USA, 2003.
36. Whitehouse, M.J.; Kemp, A.I.S. On the difficulty of assigning crustal residence, magmatic protolith and metamorphic ages to Lewisian granulites: Constraints from combined in situ U–Pb and Lu–Hf. In *Continental Tectonics and Mountain Building: The Legacy of Peach and Horne*; Special Publications, 335; Law, R.D., Butler, R.W.H., Holdsworth, R.E., Krabbendam, M., Strachan, R.A., Eds.; Geological Society: London, UK, 2010; pp. 79–99.
37. Kemp, A.I.S.; Hawkesworth, C.J. Growth and Differentiation of the Continental Crust from Isotope Studies of Accessory Minerals. In *Treatise on Geochemistry*, 2nd ed.; Holland, H.D., Turekian, K.K., Eds.; Elsevier Inc.: Amsterdam, The Netherlands, 2014; Volume 4, pp. 379–421.
38. Nemchin, A.A.; Pidgeon, R.T.; Whitehouse, M.J. Re-evaluation of the origin and evolution of> 4.2 Ga zircons from the Jack Hills metasedimentary rocks. *Earth Planet. Sci. Lett.* **2006**, *244*, 218–233. [CrossRef]
39. Whitehouse, M.J.; Nemchin, A.A. High precision, high accuracy measurement of oxygen isotopes in a large lunar zircon by SIMS. *Chem. Geol.* **2009**, *261*, 32–42. [CrossRef]
40. Kemp, A.I.S.; Hawkesworth, C.J.; Collins, W.J.; Gray, C.M.; Blevin, P.L. Isotopic evidence for rapid continental growth in an extensional accretionary orogen: The Tasmanides, eastern Australia. *Earth Planet. Sci. Lett.* **2009**, *284*, 455–466. [CrossRef]
41. Scherer, E.; Münker, C.; Mezger, K. Calibration of the lutetium-hafnium clock. *Science* **2001**, *293*, 683–687. [CrossRef] [PubMed]
42. Bouvier, A.; Vervoort, J.D.; Patchett, P.J. The Lu-Hf and Sm-Nd isotopic composition of CHUR: Constraints from unequilibrated chondrites and implications for the bulk composition of terrestrial planets. *Earth Planet. Sci. Lett.* **2008**, *273*, 48–57. [CrossRef]
43. Middlemost, E.A.K. Naming materials in the magma/igneous rock system. *Earth-Sci. Rev.* **1994**, *37*, 215–224. [CrossRef]
44. Taylor, S.R.; McLennan, S.M. *The Continental Crust: Its Composition and Evolution*; Blackwell: London, UK, 1985; p. 312.
45. Sun, S.S.; McDonough, W.F. Chemical and isotopic systematics of oceanic basalts: Implications for mantle composition and processes. In *Magmatism in Ocean Basins*; Sauders, A.D., Norry, M.J., Eds.; Geological Society of London: London, UK, 1989; Volume 42, pp. 313–345.
46. Dhuime, B.; Hawkesworth, C.J.; Storey, C.D.; Cawood, P.A. From sediments to their source rocks: Hf and Nd isotopes in recent river sediments. *Geology* **2011**, *39*, 407–410. [CrossRef]
47. Valley, J.W.; Kinny, P.D.; Schulze, D.J.; Spicuzza, M.J. Zircon megacrysts from kimberlite: Oxygen isotope variability among mantle melts. *Contrib. Mineral. Petrol.* **1998**, *133*, 1–11. [CrossRef]
48. Albert, C. Archean Evolution of the Southern Sao Francisco Craton (SE Brazil). Ph.D. Thesis, Universidade Federal de Ouro Preto, Ouro Preto, Brazil, 2017.
49. Valley, J.W.; Lackey, J.S.; Cavosie, A.J.; Clechenko, C.C.; Spicuzza, M.J.; Basei, M.A.S.; Bindeman, I.N.; Ferreira, V.P.; Sial, A.N.; King, E.M.; et al. 4.4 billion years of crustal maturation: Oxygen isotope ratios of magmatic zircon. *Contrib. Mineral. Petrol.* **2005**, *150*, 561–580. [CrossRef]
50. Kemp, A.I.S.; Hawkesworth, C.J.; Paterson, B.A.; Kinny, P. Episodic growth of the Gondwana supercontinent from hafnium and oxygen isotopes in zircon. *Nature* **2006**, *439*, 580–583. [CrossRef]
51. Wang, S.J.; Wan, Y.S.; Zhang, C.J.; Yang, E.X.; Song, Z.Y.; Wang, L.F.; Zhang, F.Z. Major advanced development gained in studying early Precambrian geology in the Luxi area. *Shandong Land Resour.* **2008**, *24*, 10–20.
52. Wang, C.Y.; Campbell, I.H.; Stepanov, A.S.; Allen, C.M.; Burtsev, I.N. Growth rate of the preserved continental crust: II. Constraints from Hf and O isotopes in detrital zircons from Greater Russian Rivers. *Geochim. Cosmochim. Acta* **2011**, *75*, 1308–1345. [CrossRef]
53. Pietranik, A.B.; Hawkesworth, C.J.; Storey, C.D.; Kemp, A.I.S.; Sircombe, K.N.; Whitehouse, M.J.; Bleeker, W. Episodic, mafic crust formation from 4.5 to 2.8 Ga: New evidence from detrital zircons, Slave craton, Canada. *Geology* **2008**, *36*, 875–878. [CrossRef]
54. Dhuime, B.; Hawkesworth, C.J.; Cawood, P.A.; Storey, C.D. A change in the geodynamics of continental growth 3 billion years ago. *Science* **2012**, *335*, 1334–1336. [CrossRef]
55. Lancaster, P.J.; Storey, C.D.; Hawkesworth, C.J. The Eoarchean foundation of the North Atlantic Craton. In *Continent Formation Through Time*; Roberts, N.M.W., van Kranendonk, M., Parman, S., Shirey, S., Clift, P.D., Eds.; Geological Society of London, Special Publications: London, UK, 2014; pp. 261–279.
56. Rapaela, C.W.; Fanning, C.M.; Casquet, C.; Pankhurst, R.J.; Spalletti, L.; Poiré, D.; Baldo, E.G. The Rio de la Plata craton and the adjoining Pan-African/brasiliano terranes: Their origins and incorporation into south-west Gondwana. *Gondwana Res.* **2011**, *20*, 673–690. [CrossRef]
57. Almeida, F.F.M.; Hasui, Y.; Brito Neves, B.B.; Fuck, R.A. Brazilian structural provinces: An introduction. *Earth-Sci. Rev.* **1981**, *17*, 1–29. [CrossRef]
58. Pimentel, M.M.; Fuck, R.A. Neoproterozoic crustal accretion in central Brazil. *Geology* **1992**, *20*, 375–379. [CrossRef]
59. Strieder, A.J.; Suita, M.T.F. Neoproterozoic geotectonic evolution of Tocantins Structural Province, central Brazil. *J. Geodyn.* **1999**, *28*, 267–289. [CrossRef]

60. Pimentel, M.M. The tectonic evolution of the Neoproterozoic Brasília Belt, central Brazil: A geochronological and isotopic approach. *Braz. J. Geol.* **2016**, *46*, 67–82. [CrossRef]
61. Araújo Filho, J.O. The Pirineus Syhntaxis: An example of the intersection of two Brasiliano foldthrust belts in central Brazil and its implications for the tectonic evolution of western Gondwana. *Braz. J. Geol.* **2000**, *30*, 144–148.
62. Fuck, R.A.; Pimentel, M.M.; Silva, L.J.H.D.R. Compartimentação Tectônica na porção oriental da Província Tocantins. In Proceedings of the 38th Brazilian Congress of Geology, SBG, Balneário de Camboriú, Brazil, 23–28 October 1994; Volume 38, pp. 215–216.
63. Dardenne, M.A. The Brasília fold belt. In Proceedings of the Tectonic Evolution of South America, 31st International Geological Congress, Rio de Janeiro, Brazil, 6–17 August 2000; pp. 231–236.
64. Valeriano, C.M.; Machado, N.; Simonetti, A.; Valladares, C.S.; Seer, H.J.; Simões, L.S.A. U-Pb geochronology of the southern Brasília belt (SE-Brazil): Sedimentary provenance, Neoproterozoic orogeny and assembly of West Gondwana. *Precis. Res.* **2004**, *130*, 27–55. [CrossRef]
65. Valeriano, C.M.; Pimentel, M.M.; Heilbron, M.; Almeida, J.C.H.; Trouw, R.A. *Tectonic Evolution of the Brasília Belt, Central Brazil, and Early Assembly of Godwana*; Special Publications, Geological Society: London, UK, 2008; Volume 294, pp. 197–210.
66. Costa, L.A.M.; Portela, A.C.; Nilson, A.A.; Vale, C.R.O.; Marchetto, C.L.M.; Santos, E.L.; Meneguesso, G.; Inda, H.A.V.; Sterna, R.; Marchetto, M.; et al. *Projeto Leste do Tocantins/Oeste do São Francisco*; Final Report; Convênio DNPM/CPRM/PROSPEC: Rio de Janeiro, Brazil, 1976; p. 200.
67. Padilha, J.L. Prospecção de ouro na região nordeste de Goiás-Projeto Pindorama-Docegeo. In Proceedings of the 1st Regional Meeting of Gold in Goiás, Brazil, 1984; pp. 78–95.
68. Ferreira Filho, C.F.; Pimentel, M.M.; Araujo, S.M.; Laux, J. Layered Intrusions and Volcanic Sequences in Central Brazil: Geological and Geochronological Constraints for Mesoproterozoic (1.25 Ga) and Neoproterozoic (0.79 Ga) Igneous Associations. *Precis. Res.* **2010**, *183*, 617–634. [CrossRef]
69. Piuzana, D.; Pimentel, M.M.; Fuck, R.A.; Armstrong, R. Neoproterozoic magmatism and high-grade metamorphism in the Brasília Belt, central Brazil: Regional implications of SHRIMP U-Pb and Sm-Nd geochronological studies. *Precis. Res.* **2003**, *125*, 245–273. [CrossRef]
70. Pimentel, M.M.; Fuck, R.A.; Gioia, S.M.C.L. The Neoproterozoic Goiás Magmatic Arc, Central Brazil: A review and new Sm–Nd isotopic data. *Braz. J. Geol.* **2000**, *30*, 35–39. [CrossRef]
71. Jost, H.; Fuck, R.; Brod, J.A.; Dantas, E.L.; Meneses, P.R.; Assad, M.L.P.; Pimentel, M.M.; Blum, M.L.B.; Silva, A.M.; Spigolon, A.L.D.; et al. Geologia dos terrenos arqueanos e proterozóicos da região de Crixás-Cedrolina, Goiás. *Braz. J. Geol.* **2001**, *31*, 315–328.
72. Queiroz, C.L. Evolução Tectono-Estrutural dos Terrenos Granito-Greenstone Belt de Crixás, Brasil Central. Ph.D. Thesis, University of Brasília, Brasília, Brazil, 2000.
73. Delgado, I.M.; Souza, J.D.; Silva, L.C.; Silveira Filho, N.C.; Santos, R.A.; Pedreira, A.J.; Guimarães, J.T.; Angelim, L.A.; Vasconcelos, A.M.; Gomes, I.P.; et al. Província Tocantins. In *Geologia, Tectônica e Recursos Minerais do Brasil*; Bizzi, L.A., Schobbenhaus, C., Vidotti, R.M., Gonçalves, J.H., Eds.; CPRM: Rio de Janeiro, Brazil, 2003; pp. 281–292.
74. Jost, H.; Chemale, F., Jr.; Dussin, I.A.; Tassinari, C.C.G.; Martins, R. A U-Pb zircon Paleoproterozoic age for the metasedimentary host rocks and gold mineralization of the Crixás greenstone belt, Goiás, Central Brazil. *Ore Geol. Rev.* **2010**, *37*, 127–139. [CrossRef]
75. Jost, H.; Dussin, I.A.; Chemale, F., Jr.; Tassinari, C.C.G.; Junges, S. U-Pb and Sm-Nd constrains for the Paleoproterozoic age of the metasedimentary sequences of the Goiás Archean greenstone belts. In Proceedings of the 6th South American Symposium on Isotope Geology, San Carlos de Bariloche, Argentina, 13–17 April 2008; p. 4.
76. Jost, H.; Rodrigues, V.G.; Carvalho, N.J.; Chemale, F., Jr.; Marques, J.C. Estratigráfica e geocronologia do greenstone belt de Guarinos, Goiás. *Geol. USP Série Científica* **2012**, *12*, 3–48.
77. Borges, C.C.A.; Toledo, C.L.B.; Silva, A.M.; Chemale, F., Jr.; Host, H.; Lana, C.C. Geochemistry and isotopic signatures of metavolcanic and metaplutonic rocks of the Faina and Serra de Santa Rita greenstone belts, Central Brazil: Evidences for a Mesoarchean intraoceanic arc. *Precis. Res.* **2017**, *292*, 350–377. [CrossRef]
78. Corrêa da Costa, P.C. Petrologia, Geoquímica, e Geocronologia dos Diques Máficos da Região de Crixás-Goiás, Porção Centro-Oeste do Estado de Goiás. Ph.D. Thesis, University of São Paulo, São Paulo, Brazil, 2003.
79. Blum, M.L.B.; Jost, H.; Moraes, R.A.V.; Pires, A.C.B. Caracterização dos complexos ortognáissicos arqueanos de goiás por gamaespectrometria aérea. *Braz. J. Geol.* **2003**, *33* (Suppl. 2), 147–152. [CrossRef]
80. Danni, J.C.M.; Ribeiro, C.C. Caracterização Estratigráfica da Sequência Vulcanosedimentar de Pilar de Goiás e de Guarinos, Goiás. In Proceedings of the 30th Brazilian Congress of Geology, Recife, Brazil, 1978; Volume 2, pp. 582–596.
81. Sabóia, L.A. Os 'Greenstone Belts' de Crixás e Goiás, GO. *Bol. Inf. NCO* **1979**, *9*, 43–72.
82. Resende, M.G.; Jost, H.; Osborne, G.A.; Mol, A.G. Stratigraphy of the Goiás and Faina greenstone belts, Central Brazil: A new proposal. *Braz. J. Geol.* **1998**, *28*, 77–94. [CrossRef]
83. Brant, R.A.P.; Souza, V.S.; Dantas, E.L.; Jost, H.; Rodrigues, V.G.; Carvalho, M.J.; Araújo, K.C. Contribuição ao estudo de proveniência sedmentar com base em dados U-Pb para o greenstone belt de Faina, Goiás. In Proceedings of the SBG, 14th Simpósio de Geologia do Centro-Oeste, Brasília, Brazil, 6–9 September 2015; pp. 30–33.

84. Salles, R.R.; Costa, D.A.; Appollo, J.; Lunkes, M.; Santos, B.; Jost, H.; Massucatto, A.J. The first spinifex occurrence at Mina Inglesa sequence, Crixás greenstone belt, Crixás, Goiás, Brazil. In Proceedings of the 47th Brazilian Congress of Geology, Salvador, Brazil, 23 September 2014. Abstracts in CD.
85. Tomazzoli, E.R. Geologia, Petrologia, Deformação e Potencial Aurífero do Greenstone Belt de Goiás—GO. Master's Thesis, University of Brasília, Brasília, Brazil, 1985.
86. Profumo, J.J.L. Alteração Hidrotermal das Rochas Ultramáficas e Máficas do Greenstone Belt de Goiás Velho, GO. Master's Thesis, University of Brasília, Brasília, Brazil, 1993.
87. Fortes, P.T.F.O.; Pimentel, M.M.; Santos, R.V.; Junges, S.L. Sm-Nd studies at Mina III gold deposit, Crixás greenstone belt, Central Brazil: Implications for the depositional age of the upper metasedimentary rocks and associated Au mineralization. *J. South Am. Earth Sci.* **2003**, *16*, 503–512.
88. Theodoro, S.C. Ambiente de Sedimentação da Formação Ribeirão das Antas, Grupo Crixás, Goiás, Brasil. Master's Thesis, University of Brasília, Brasília, Brazil, 1995.
89. Resende, M.G.; Jost, H. Redefinição da Formação Aimbé, greenstone belt de Guarinos, Goiás e sua interpretação paleogeográfica e paleotectônica. SBG. *Bol. Geoc. Centro-Oeste* **1994**, *17*, 49–57.
90. Jost, H.; Kuyumjian, R.M.; Freitas, A.L.S.; Costa, A.L.L.; Nascimento, C.T.C.; Vasconcelos, F.M.; Galotti Neto, L.; Martins, M.C.; Carvalho, M.N.; Condé, V.C. Geologia da porção norte do greenstone belt de Guarinos, Goiás. *Braz. J. Geol.* **1995**, *25*, 51–60. [CrossRef]
91. Danni, J.C.M.; Dardenne, M.A.; Fuck, R.A. Geologia da região da Serra da Santa Rita e Sequência Serra de Cantagalo. In Proceedings of the SBG, Simpósio de Geologia do Centro-Oeste, Goiânia, Brazil, 25–31 October 1981; pp. 265–280.
92. Teixeira, A.S. Geologia da região de Goiás-Faina. In Proceedings of the SBG, Simpósio de Geologia do Centro-Oeste, Goiânia, Brazil, 25–31 October 1981; pp. 344–360.
93. Resende, M.G.; Jost, H.; Lima, B.E.M.; Teixeira, A.A. Proveniência e idades modelo Sm-Nd das rochas siliciclásticas arqueanas dos greenstone belts de Faina e Santa Rita, Goiás. *Braz. J. Geol.* **1999**, *29*, 281–290.
94. Corrêa da Costa, P.C.; Girardi, V.A.V.; Teixeira, W. $^{40}Ar/^{39}Ar$ and Rb-Sr Geochronology of the Goiás-Crixás Dike Swarm, Central Brazil: Constrains on the Neoarchean-Paleoproterozoic Tectonic Boundary in South America, and Nd-Sr Signature of the Subcontinental Mantle. *Int. Geol. Rev.* **2006**, *48*, 547–560. [CrossRef]
95. Fortes, P.T.F.O. Metalogênese dos Depósitos Auríferos Mina III, Mina Nova e Mina Inglesa, Greenstone Belt de Crixás, GO. Ph.D. Thesis, University of Brasília, Brasília, Brazil, 1996.
96. Santos, R.V.; Oliveira, C.G.; Souza, V.H.V.; Carvalho, M.J.; Andrade, T.V.; Souza, H.G.A. Correlação isotópica baseada em isótopos de Carbono entre os greenstone belts de Goiás. In Proceedings of the 44th Brazilian Congress of Geology, Curitiba, Brazil, 26–31 October 2008; p. 52.
97. Melezhik, V.A.; Huhma, H.; Condon, D.J.; Fallick, A.E.; Whitehouse, M.J. Temporal constraints on the Paleoproterozoic Lomagundi-Jatuli carbon isotopic event. *Geology* **2007**, *35*, 655. [CrossRef]
98. Jost, H.; Ferreia Filho, C.F. *Geologia da Região Meridional do Greenstonebelt de Guarinos, GO*; Internal Report; Institute of Geosciences, University of Brasília: Brasília, Brazil, 1987.
99. Magalhães, L.F. Cinturão de Cisalhamento de Empurrão Córrego Geral/Meia Pataca: Geologia, Deformação, Alteração Hidrotermal e Mineralizações Auríferas Associadas (Crixás, Goiás). Master's Thesis, University of Brasília, Brasília, Brazil, 1991.
100. Queiroz, C.L. Caracterização dos Domínios Estruturais e da Arquitetura do Greenstone Belt de Crixás, Go. Master's Thesis, University of Brasília, Brasília, Brazil, 1995.
101. Queiroz, C.L.; Jost, H.; McNaughton, N. U–Pb-SHRIMP ages of Crixás granite-greenstone belt terranes: From Archaean to Neoproterozoic. Resumos Expandidos. In Proceedings of the 7th Simpósio Nacional de Estudos Tectônicos, Lençóis, Brazil, 28 May–1 June 2001.
102. Thomson, M.L. Wall-rock alteration related to Au mineralization in the low amphibolite facies: Crixás Gold Mine, Goiás, Brazil. *Can. Mineral.* **1991**, *29*, 461–480.
103. Carvalho, R.S. *Mapeamento Geológico Estrutural da Faixa Leste-Oeste ao Norte do Greenstone Belt de Crixás (GO)*; Institute of Geoscience, University of Rio de Janeiro: Rio de Janeiro, Brazil, 2005; Unpublished report.
104. Sobiesiak, M.S. Caracterização de Depósito Aurífero no Corpo Pequizão, Crixás-GO. Bachelor's Thesis, Institute of Geoscience, Federal University of Rio Grande do Sul, Porto Alegre, Brazil, 2011. Unpublished.
105. Sibson, R.H. Generation of pseudotachylyte by ancient seismic faulting. *Geophys. J. R. Astron. Soc.* **1975**, *43*, 775–794. [CrossRef]
106. Bogossian, J.; Hagemann, S.G.; Rodrigues, V.G.; Lobato, L.M.; Roberts, M. Hydrothermal alteration and mineralization in the Faina greenstone belt: Evidence from the Cascavel and Sertão orogenic gold deposits. *Ore Geol. Rev.* **2020**, *119*, 103293. [CrossRef]
107. Petersen, K.J., Jr. Estudo das Mineralizações dos Corpos IV e V da Estrutura IV do Greenstone Belt de Crixás (GO). Ph.D. Thesis, University of São Paulo, São Paulo, Brazil, 2003.
108. Massucato, A.J. *Relatório de Geologia Estrutural—Aspectos Estruturais do Greenstone Belt de Crixás—GO—Anglogold Ashanti, Crixás-GO*; AngloGold Ashanti: Johannesburg, South Africa, 2004; p. 30, Unpublished Internal Report.
109. Jost, H.; Pimentel, M.M.; Fuck, R.A.; Danni, J.C.; Heaman, L. Idade U-Pb do Diorito Posselândia, Hidrolina, Goiás. *Braz. J. Geol.* **1993**, *23*, 352–355. [CrossRef]
110. Jost, H.; Oliveira, A.M.; Vargas, M.C. Petrography, geochemistry and structural control of trondhjemitic intrusions in greenstone belts of the Crixás region. In Proceedings of the 37th Brazilian Congress of Geology, São Paulo, Brazil, 1992; Volume 1, pp. 43–44.

111. Araújo Filho, J.O.; Kuyumjian, R.M. Structurally controlled gold occurrences in the Brasília fold-thrust belt of central and SE-Goiás. *Braz. J. Geol.* **2000**, *30*, 289–292. [CrossRef]
112. Alkmim, F.F.; Marshak, S. Transamazonian Orogeny in the Southern São Francisco Craton Region, Minas Gerais Brazil: Evidence for a Paleoproterozoic collision and collapse in Quadrilátero Ferrífero. *Precis. Res.* **1998**, *90*, 29–58. [CrossRef]
113. Goldfarb, R.J.; Baker, T.; Dube, B.; Groves, D.I.; Hart, C.J.R.; Gosselin, P. *Distribution, Character, and Genesis of Gold Deposits in Metamorphic Belts*; Society of Economic Geologists: Littleton, CO, USA, 2005; pp. 407–450.
114. Groves, D.I.; Goldfarb, R.J.; Knox-Robinson, C.M.; Ojala, J.; Gardoll, S.; Yun, G.Y.; Holyland, P. Late-kinematic timing of orogenic gold deposits and significance for computer-based exploration techniques with emphasis on the Yilgarn Block, Western Australia. *Ore Geol. Rev.* **2000**, *17*, 1–38. [CrossRef]
115. Orinoco Gold Limited. Available online: http://orinocogold.com/cgi-sys/suspendedpage.cgi (accessed on 19 January 2021).
116. Fortes, P.T.F.O.; Coelho, R.F.; Giuliani, G. Au;Ag ratio variations at Mina III, Mina Nova and Mina Inglesa gold deposits, Crixás greenstone belt, Brazil. *Braz. J. Geol.* **2000**, *30*, 246–250.
117. Coelho, R.F. Caracterização Mineralógica de Minérios das Jazidas Auríferas Mina III e Mina Nova, Greenstone Belt de Crixás (GO). Master's Thesis, University of Brasília, Brasília, Brazil, 1990.
118. Fortes, P.T.F.O. Geologia do Depósito Aurífero Mina III, Crixás, Goiás. Master's Thesis, University of Brasília, Brasília, Brazil, 1991.
119. Souza, J.J. Geologia e Exploração de Pilar, a Próxima Mina da Yamana Gold no Estado de Goiás. In Proceedings of the Yamana Gold Presentation at SIMEXMIN, Ouro Preto, Brazil, 12–20 May 2012; p. 33.
120. Orinoco Gold Limited (ASX:OGX), 2014 to 2018. Annual Reports. Available online: https://orinocogold.com/shareholder-centre/financial-reports/annual-reports (accessed on 19 January 2021).
121. Pulz, G.M. Modelos Prospectivos para Ouro em Greenstone Belts: Exemplo dos Depósitos Maria Lázara e Ogó, na Região de Guarinos e Pilar de Goiás, Goiás. Ph.D. Thesis, University of Brasília, Brasília, Brazil, 1995.
122. Sibson, R.H. Conditions for fault-valve behaviour. In *Deformation Mechanisms, Rheology and Tectonics*; Knipe, R.J., Rutter, E.H., Eds.; Special Publication, Geological Society of London: London, UK, 1990; Volume 54.
123. Michel, D.; Giuliani, G.; Pulz, G.M.; Jost, H. Multistage gold deposition in the Archaean Maria Lázara gold deposit (Goiás, Brazil). *Minim. Depos.* **1994**, *29*, 94–97. [CrossRef]
124. Thomson, M.L. The Crixás Gold Deposit; Brazil: Metamorphism, Metassomatism and Gold Mineralization. Ph.D. Thesis, University of Western Ontario, London, ON, Canada, 1987.
125. Thomson, M.L.; Fyfe, W.S. The Crixás gold deposit, Brazil: Thrustrelated postpeak metamorphic gold mineralization of possible Brasiliano cycle age. *Econ. Geol.* **1990**, *85*, 928–942. [CrossRef]
126. Okamoto, H.; Massalki, T.B. The Au-Bi (Gold-Bismuth) System. *Bull. Alloy Phase Diagr.* **1983**, *4*, 401–407. [CrossRef]
127. Patchett, P.J. Importance of the Lu–Hf isotope system in studies of planetary chronology and chemical evolution. *Geochim. Cosmochim. Acta* **1983**, *47*, 81–91. [CrossRef]
128. Brown, K.L. Gold deposition from geothermal discharge in New Zealand. *Econ. Geol.* **1986**, *81*, 979–983. [CrossRef]
129. Seward, T.M. The hydrothermal chemistry of gold and its implications for ore formations: Boiling and conductive cooling as examples. In *The Geology of Gold Deposits: The Perspective in 1988*; Keays, R.R., Ramsay, W.R.H., Groves, D.I., Eds.; Economic Geology Monograph 6; Society of Economic Geologists: Littleton, CO, USA, 1989; pp. 398–404.
130. Sibson, R.H.; Robert, F.; Poulsen, K.H. High-angle reverse faults, fluid pressure cycling, and mesothermal gold-quartz deposits. *Geology* **1988**, *16*, 551–555. [CrossRef]
131. Robert, F.; Boullier, A.-M.; Firclaous, F. Gold-quartz veins in metamorphic terranes and their bearing on the role of fluids in faulting. *J. Geoph. Res.* **1995**, *100*, 12861–12879. [CrossRef]
132. Dugdale, A.L.; Hagemann, S.G. The Bronzewing lode-gold deposit, Western Australia: P-T-X evidence for fluid immiscibility caused by cyclic decompression in gold-bearing quartz-veins. *Chem. Geology* **2001**, *173*, 59–90. [CrossRef]
133. Fortes, P.T.F.O.; Cheilletz, A.; Giuliani, G.; Féraud, G. A Brasiliano age (500 ± 5 Ma) for the Mina III gold deposit, Crixás Greenstone Belt, Central Brazil. *Int. Geol. Rev.* **1997**, *39*, 449–460. [CrossRef]
134. Tassinari, C.C.G.; Jost, H.; Santos, J.C.; Nutman, A.P.; Bennell, M.R. Pb and Nd isotope signatures and SHRIMP U-Pb geochronological evidence of Paleoproterozoic age for Mina III gold mineralization, Crixás District, Central Brazil. In Proceedings of the 5th South American Symposium on Isotope Geology, Punta Del Este, Uruguay, 24–27 April 2006; pp. 527–529.
135. Carvalho, M.J.; Rodrigues, V.G.; Jost, H. Formação Arraial Dantas: Depósito aurífero detrítco glaciogênico do greentone belt de Faina, Goiás. In Proceedings of the 3rd Brazilian Symposium on Metallogeny, Gramado, Brazil, 2–5 June 2013; p. 2.
136. Teixeira, J.B.G.; Silva, M.G.; Misi, A.; Cruz, S.C.P.; Sá, J.H.S. Geotectonic and metallogeny of the northern São Francisco craton, Bahia, Brazil. *J. South Am. Earth Sci.* **2010**, *30*, 71–83. [CrossRef]
137. Arndt, N.T.; Goldstein, S.L. Use and abuse of crust-formation ages. *Geology* **1987**, *15*, 893–895. [CrossRef]
138. Hammerli, J.; Kemp, A.I.S.; Spandler, C. Neodymium isotope equilibration during crustal metamorphism revealed by in situ microanalysis of REE-rich accessory minerals. *Earth Planet. Sci. Lett.* **2014**, *392*, 133–142. [CrossRef]
139. Bauer, A.M.; Fisher, C.; Vervoort, J.; Bowring, S. The Role of accessory phases in the Sm-Nd isotope systematics of the Acasta Gneiss Complex. In Proceedings of the 2015 Fall Meeting, AGU, San Francisco, CA, USA, 14–18 December 2015. Abstract V43D-07.

140. Vervoort, J.D.; Kemp AI, S. Clarifying the zircon Hf isotope record of crust-mantle evolution. *Chem. Geol.* **2016**, *425*, 65–75. [CrossRef]
141. Amelin, Y.; Lee, D.C.; Halliday, A.N.; Pidgeon, R.T. Nature of the Earth's earliest crust from hafnium isotopes in single detrital zircons. *Nature* **1999**, *399*, 252–255. [CrossRef]
142. DeCelles, P.G.; Ducea, M.N.; Kapp, P.; Zandt, G. Cyclicity in Cordilleran orogenic systems. *Nat. Geosci.* **2009**, *2*, 251–257. [CrossRef]
143. Collins, W.J.; Belousova, E.A.; Kemp, A.I.S.; Murphy, J.B. Two contrasting Phanerozoic orogenic systems revealed by hafnium isotope data. *Nat. Geosc.* **2011**, *4*, 333–337. [CrossRef]
144. Silver, L.T.; Deutsch, S. Uranium–lead isotopic variations in zircon: A case study. *J. Geol.* **1963**, *71*, 721–758. [CrossRef]
145. Pidgeon, R.T.; O'Neill, J.R.; Silver, R.T. Uranium and lead isotopic stability in a metamict zircon under experimental hydrothermal conditions. *Science* **1966**, *154*, 1538–1540. [CrossRef]
146. Pimentel, M.M.; Dantas, E.L.; Fuck, R.A.; Armstrong, R.A. SHRIMP and conventional U-Pb age, sm-Nd isotopic characteristics and tectonic significance of the K-rich Itapuranga suite in Goiás, Central Brazil. *Proc. Braz. Acad. Sci.* **2003**, *75*, 97–108. [CrossRef]
147. Pimentel, M.M.; Fuck, R.A.; Silva, L.J.H.D. Dados Rb–Sr e Sm–Nd da região de Jussara-Goiás-Mossâmedes (GO), e o limite entre terrenos antigos do Maciço de Goiás e o Arco Magmático de Goiás. *Braz. J. Geol.* **1996**, *26*, 61–70. [CrossRef]
148. Guimarães, S.B.; Moura, M.A.; Dantas, E.L. Petrology and geochronology of Bom Jardim copper deposit. *Braz. J. Geol.* **2012**, *42*, 841–862.
149. Marques, G.C. Evolução Tectônica e Metalogenética no Contexto do Depósito Aurífero de Fazenda Nova, Arco Magmático de Arenópolis, Goiás. Ph.D. Thesis, University of Brasília, Brasília, Brazil, 2017.
150. Arndt, N.T.; Teixeira, N.A.; White, W.M. Bizarre geochemistry of komatiites from the Crixás Greenstone Belt. *Contr. Mineral. Petrol.* **1989**, *101*, 187–197. [CrossRef]
151. Lacerda Filho, J.V.; Rezende, A.; Silva, A. *Programa Levantamentos Geológicos Básicos: Geologia e Recursos Minerais do Estado de Goiás e Distrito Federal, Escala 1, 500.000*; CPRM: Goiânia, Brazil, 2000.
152. Kuyumjian, R.M.; Teixeira, N.A. Um novo tipo de estrutura em lavas ultramáficas: Greenstone belt de Crixás, GO. *Braz. J. Geol.* **1982**, *12*, 572–577. [CrossRef]
153. Jost, H.; Brod, J.A.; Kuyumjian, R.M. Aspectos geoquímicos de metabasaltos do greenstone belt de Guarinos, Goiás. *Braz. J. Geol.* **1999**, *29*, 449–451.
154. Kemp, A.I.S.; Hawkesworth, C.J. Granitic perspectives on the generation and secular evolution of the continental crust. In *The Crust, Treatise in Geochemistry*; Rudnick, R.L., Ed.; Elsevier: Amsterdam, The Netherlands, 2003; Volume 3, pp. 349–410.
155. Smithies, R.H.; Champion, D.C.; Van Kranendonk, M.J. Formation of Paleoarchean continental crust through infracrustal melting of enriched basalt. *Earth Planet. Sci. Lett.* **2009**, *281*, 298–306. [CrossRef]
156. Condie, K.C.; Aster, R.C. Episodic zircon age spectra of orogenic granitoids: The supercontinent connection and continental growth. *Precis. Res.* **2010**, *180*, 227–236. [CrossRef]
157. Kamber, B.S. The evolving nature of terrestrial crust from the Hadean, through the Archaean, into the Proterozoic. *Precis. Res.* **2015**, *258*, 48–82. [CrossRef]
158. Drummond, M.S.; Defant, M.J. A model for trodhjemite–tonalite–dacite genesis and crustal growth via slab melting: Archaen to modern comparisons. *J. Geophys. Res.* **1990**, *95*, 21503–21521. [CrossRef]
159. Moyen, J.-F. The composite Archaean grey gneisses: Petrological significance, and evidence for a non-unique tectonic setting for Archaean crustal growth. *Lithos* **2011**, *123*, 21–36. [CrossRef]
160. Hollings, P.; Wyman, D. Trace element and Sm-Nd systematics of volcanic and intrusive rocks from the 3 Ga Lumby Lake Greenstone belt, Superior Province: Evidence for Archean pluma-arc interaction. *Lithos* **1999**, *46*, 189–213. [CrossRef]
161. Van Kranendonk, M.J.; Smithies, R.H.; Griffin, W.L.; Huston, D.L.; Hickman, A.H.; Champion, D.C.; Anhaeusser, C.R.; Pirajno, F. *Making It Thick: A Volcanic Plateau Origin of Paleoarchean Continental Lithosphere of the Pilbara and Kaapval Cratons*; Special Publications, Geological Society of London: London, UK, 2015; Volume 389, pp. 83–111.
162. Rey, P.F.; Philippot, P.; Thébaud, N. Contribution of mantle plumes, crustal thickening and greenstone blanketing to the 2.75–2.65 Ga global crisis. *Precis. Res.* **2003**, *127*, 43–60. [CrossRef]
163. Stern, R.J. Evidence from ophiolites, blueschists, and ultrahigh-pressure metamorphic terranes that the modern episode of subduction tectonics began in Neoproterozoic time. *Geology* **2005**, *33*, 557–560. [CrossRef]
164. Bédard, J.H. A catalytic delamination-driven model for coupled genesis of Archean crust and sub-continental lithospheric mantle. *Geoch. Cosm. Acta* **2006**, *70*, 1188–1214. [CrossRef]
165. Shirey, S.B.; Richardson, S.H. Start of the Wilson cycle at 3 Ga shown by diamonds from subcontinental mantle. *Science* **2011**, *333*, 434–436. [CrossRef]
166. Van Kranendonk, M.J. Onset of plate tectonics. *Science* **2011**, *333*, 413–414. [CrossRef]
167. Wyman, D.A. A critical assessment of Neoarchean "plume only" geodynamics: Evidence from the Superior Province. *Precis. Res.* **2013**, *229*, 3–19. [CrossRef]
168. Arndt, N.T. Komatiites. In *Archean Crustal Evolution*; Condie, K.C., Ed.; Elsevier: Amsterdam, The Netherlands, 1994; pp. 11–44.
169. Condie, K.C. High field strength element ratios in Archean basalts: A window to evolving sources of mantle plumes? *Lithos* **2005**, *79*, 491–504. [CrossRef]

170. Barnes, S.J.; Van Kranendonk, M.J. Archean andesites in the east Yilgarn craton, Australia: Products of plume-crust interaction? *Lithosphere* **2014**, *6*, 80–92. [CrossRef]
171. Willbold, M.; Hegner, E.; Stracke, A.; Rocholl, A. Continental geochemical signatures in dacites from Iceland and implications for models of early Archaean crust formation. *Earth Planet. Sci. Lett.* **2009**, *279*, 44–52. [CrossRef]
172. Hollings, P.; Kerrich, R. Trace element systematics of ultramafic and mafic volcanic rocks from the 3 Ga North Caribou greenstone belt, northwestern Superior Province. *Precis. Res.* **1999**, *93*, 257–279. [CrossRef]
173. Fralick, P.; Hollings, P.; King, D. *Stratigraphy, Geochemistry, and Depositional Environments of Mesoarchean Sedimentary Units in Western Superior Province; Implications for Generation of Early Crust*; Geological Society of America Special Paper 440; Geological Society of America: Boulder, CO, USA, 2008; pp. 77–96.
174. François, C.; Philippot, P.; Rey, P.; Rubatto, D. Burial and exhumation during Archean sagduction in the East Pilbara granite-greenstone terrane. *Earth Planet. Sci. Lett.* **2014**, *396*, 235–251. [CrossRef]
175. Tomlinson, K.Y.; Stevenson, R.K.; Hughes, D.J.; Hall, R.P.; Thurston, P.C.; Henry, P. The Red Lake green-stone belt, Superior Province: Evidence of plume-related magmatism at 3 Ga and evidence of an older enriched source. *Precis. Res.* **1998**, *89*, 59–76. [CrossRef]
176. Percival, J.A.; Skulski, T.; Sanborn-Barrie, M.; Stott, G.M.; Leclair, A.D.; Corkery, M.T.; Boily, M. Geology and tectonic evolution of the Superior Province, Canada. In *Tectonic Styles in Canada: The LITHOPROBE Perspective*; Special Paper 49; Percival, J.A., Cook, F.A., Clowes, R.M., Eds.; Geological Association of Canada: St. John's, NL, Canada, 2012; pp. 321–378.
177. Arndt, N. Formation and Evolution of the Continental Crust. *Geoch. Perspec.* **2013**, *2*, 405–533. [CrossRef]
178. Moyen, J.F.; Stevens, G. Experimental constraints on TTG petrogenesis: Implications for Archean geodynamics. In *Archean Geodynamics and Environments*; Benn, K., Mareschal, J.-C., Condie, K.C., Eds.; AGU: Washington, DC, USA, 2006; pp. 149–178.
179. Martin, H.; Moyen, J.-F.; Guitreau, M.; Blichert-Toft, J.; Le Pennec, J.-L. Why Archean TTG cannot be generated by MORB melting in subduction zones. *Lithos* **2014**, *198–199*, 1–13. [CrossRef]
180. Guitreau, M.; Blichert-Toft, J.; Martin, H.; Mojzsis, S.J.; Albarède, F. Hafnium isotope evidence from Archean granitic rocks for deep-mantle origin of continental crust. *Earth Planet. Sci. Lett.* **2012**, *337*, 211–223. [CrossRef]
181. Jost, H.; Apollo, J.F.H.; Weber, W.; Salles, R.R.; Marques, J.C.; Massucatto, A.J.; Costa, D.A.; Santos, B.A. Stratigraphic update, paleotectonic, paleogeographic, and depositional environments of the Crixás Greenstone Belt, Central Brazil. *J. South Am. Earth Sci.* **2019**, *96*, 102329. [CrossRef]
182. Chardon, D.; Choukroune, P.; Jayananda, M. Strain patterns, décollement and incipient sagducted greenstone terrains in the Archaean Dharwar craton (South India). *J. Struct. Geol.* **1996**, *18*, 991–1004. [CrossRef]
183. Bédard, J.H.; Brouillette, P.; Madore, L.; Berclaz, A. Archaean cratonization and deformation in the northern Superior Province, Canada: An evaluation of plate tectonic versus vertical tectonic models. *Precis. Res.* **2003**, *127*, 61–87. [CrossRef]
184. Van Kranendonk, M.J.; Collins, W.J.; Hickman, A.; Pawley, M.J. Critical tests of vertical vs. horizontal tectonic models for the Archean East Pilbara GraniteGreenstone Terrane, Pilbara Craton, Western Australia. *Precis. Res.* **2004**, *131*, 173–211. [CrossRef]
185. Robin, C.M.I.; Bailey, R.C. Simultaneous generation of Archean crust and subcratonic roots by vertical tectonics. *Geology* **2009**, *37*, 523–526. [CrossRef]
186. Van Kranendonk, M.J.; Smithies, R.H.; Hickman, A.H.; Champion, D.C. Review: Secular tectonic evolution of Archean continental crust: Interplay between horizontal and vertical processes in the formation of the Pilbara Craton, Australia. *Terra Nova* **2007**, *19*, 1–38. [CrossRef]
187. Blum, M.L.B.; Pires, A.C.B.; Mendes, L.R. *Preliminary Gravity Map and 2-D Gravity and Magnetic Data Inversion of the Crixás Greenstone Belt, Goiás*; Symposium on Archean Terranes of the South American Platform of the Brazilian Geological Society: Brasília, Brazil, 1996; pp. 33–35.
188. Hickman, A.H. Archaean diapirism in the Pilbara Block, Western Australia. In *Precambrian Tectonics Illustrated*; Kröner, A., Greiling, R., Eds.; E. Schweizerbarts'che, Verlagsbuchhandlung: Stuttgart, Germany, 1984; pp. 113–127.
189. Condie, K.C. Greenstones through time. In *Archean Crustal Evolution*; Condie, K.C., Ed.; Elsevier: Amsterdam, The Netherlands, 1994; pp. 85–120.
190. Bleeker, W.; Ketchum, J.W.F.; Jackson, V.A.; Villeneuve, M.E. The Central Slave Basement Complex; Part I: Its structural topology and autochthonous cover. *Can. J. Earth Sci.* **1999**, *36*, 1083–1109. [CrossRef]
191. Polat, A.; Kerrich, R.; Wyman, D.A. The late Archean Schreiber-Hemlo and White River-Dayohessarah greenstone belts, Superior Province: Collages of oceanic plateaus, oceanic arcs, and subduction-accretion complexes. *Tectonophysics* **1998**, *289*, 295–326. [CrossRef]
192. Percival, J.A. Geology and metallogeny of the Superior Province, Canada. In *Mineral Resources of Canada: A Synthesis of Major Deposit Types, District Metallogeny, the Evolution of Geological Provinces, and Exploration Methods*; Goodfellow, W.D., Ed.; Special Publication No. 5; Geological Association of Canada, Mineral Deposits Division: St. John's, NL, Canada, 2007; pp. 903–928.
193. Polat, A.; Appel, P.W.U.; Fryer, B.; Windley, B.; Frei, R.; Samson, I.M.; Huang, H. Trace element systematics of the Neoarchean Fiskenæsset anorthosite complex and associated meta-volcanic rocks, SW Greenland: Evidence for a magmatic arc origin. *Precis. Res.* **2009**, *175*, 87–115. [CrossRef]
194. Kerrich, R.; Wyman, D.; Fan, J.; Bleeker, W. Boninite series: Low Ti-tholeiite associations from the 2.7 Ga Abitibi greenstone belt. *Earth Planet. Sci. Lett.* **1998**, *164*, 303–316. [CrossRef]
195. Wyman, D.; Ayer, J.; Devaney, J. Niobium-enriched basalts from the Wabigoon subprovince, Canada: Evidence for adakitic metasomatism above an Archean subduction zone. *Earth Planet. Sci. Lett.* **2000**, *179*, 21–30. [CrossRef]

196. Percival, J.A.; Stern, R.A.; Rayner, N. Archean adakites from the Ashuanipi Complex, eastern Superior Province, Canada: Geochemistry, geochronology and tectonic significance. *Contrib. Mineral. Petrol.* **2003**, *145*, 265–280. [CrossRef]
197. Polat, A.; Kerrich, R. Reading the geochemical fingerprints of Archean hot subduction volcanic rocks: Evidence for accretion and crustal recycling in a mobile tectonic regime. In *Archean Geodynamics and Environments*; Benn, K., Mareschal, J.-C., Condie, K.C., Eds.; AGU: Washington, DC, USA, 2006; Volume 164, pp. 189–213.
198. Parman, S.W.; Grove, S.T.; Dann, J. The production of Barberton komatiites in an Archean subduction zone. *Geoph. Res. Lett.* **2001**, *28*, 2513–2516. [CrossRef]
199. Crawford, A.J.; Falloon, T.J.; Green, D.H. Classification, petrogenesis and tectonic setting of boninites. In *Boninites and Related Rocks*; Crawford, A.J., Ed.; Unwin Hyman: London, UK, 1989; pp. 1–49.
200. Pearce, J.A.; van der Laan, S.R.; Arculus, R.J.; Murton, B.J.; Ishii, T.; Peate, D.W.; Parkinson, I.J. Boninite and harzburgite from ODP Leg 125 (Bonin-Mariana forearc): A case study of magma genesis during the initial stages of subduction. *Proc. Ocean. Drill. Program* **1992**, 623–660. [CrossRef]
201. Borges, C.C.A.; Toledo, C.L.B.; Silva, A.M.; Chemale, F., Jr.; Santos, B.A.; Figueiredo, F.L.; Zacchi, E.N.P. Unraveling a hidden Rhyacian magmatic arc through provenance of metasedimentary rocks of the Crixás greenstone belt, Central Brazil. *Precambrian Res.* **2021**, *353*, 106022. [CrossRef]
202. Kerr, A.C.; White, R.V.; Saunders, A.D. LIP reading, recognizing oceanic plateaux in the geological record. *J. Petr.* **2000**, *41*, 1041–1056. [CrossRef]
203. Wilson, J.T. A new class of faults and their bearing on continental drift. *Nature* **1965**, *207*, 343–347. [CrossRef]
204. Groves, D.I.; Batt, W.D. Spatial and temporal variations of Archaean metallogenic associations in terms of evolution of Granitoid–Greenstone Terrains with particular emphasis on the Western Australian Shield. In *Archaean Geochemistry*; Kröner, A., Hanson, G.N., Goodwin, A.M., Eds.; Springer: Berlin/Heidelberg, Germany, 1984; pp. 73–98.
205. Ispolatov, V.; Lafrance, B.; Dubé, B.; Creaser, R.; Hamilton, M. Geologic and structural setting of gold mineralization in the Kirkland Lake–Larder Lake Gold Belt, Ontario. *Econ. Geol.* **2008**, *103*, 1309–1340. [CrossRef]
206. Bateman, R.; Ayer, J.A.; Dubé, B. The Timmins–Porcupine Gold Camp, Ontario: Anatomy of an Archean Greenstone Belt and Ontogeny of Gold Mineralization. *Econ. Geol.* **2008**, *103*, 1285–1308. [CrossRef]
207. Ashley, P.M.; Dudley, R.J.; Lesh, R.H.; Marr, J.M.; Ryall, A.W. The Scuddles Cu–Zn prospect, an Archean volcanogenic massive sulfide deposit, Golden Grove District, Western Australia. *Econ. Geol.* **1988**, *83*, 918–951. [CrossRef]
208. Hannington, M.D.; Bleeker, W.; Kjarsgaard, I. Sulfide mineralogy, geochemistry, and ore genesis of Kidd Creek deposit: Part I. North, Central, and South orebodies. In *Volcanogenic Massive Sulfide Deposit, Western Abitibi Subprovince, Canada: The Giant Kidd Creek*; Hannington, M.D., Barrie, C.T., Eds.; Economic Geology Monograph; Society of Economic Geologists: Littleton, CO, USA, 1999; pp. 163–224.
209. Cantwell, N.; Cooper, M.; Meyers, J.; Martin, N.; Sainty, R. A review of the Jaguar Cu–Zn–Ag volcanogenic massive sulphide discovery and subsequent geophysical trials. *ASEG Ext. Abstr.* **2009**, *2009*, 1–11. [CrossRef]
210. Fiorentini, M.; Beresford, S.; Barley, M.; Duuring, P.; Bekker, A.; Rosengren, N.; Cas, R.; Hronsky, J. District to Camp Controls on the Genesis of Komatiite-Hosted Nickel Sulfide Deposits, Agnew-Wiluna Greenstone Belt, Western Australia: Insights from the Multiple Sulfur Isotopes. *Econ. Geol.* **2012**, *107*, 781–796. [CrossRef]
211. Khan, R.M.K.; Naqvi, S.M. Geology, geochemistry and genesis of BIF of Kushtagi schist belt, Archaean Dharwar Craton, India. *Minim. Depos.* **1996**, *31*, 123–133. [CrossRef]
212. Angerer, T.; Hagemann, S.G. The BIF-hosted high-grade iron ore deposits in the Archean Koolyanobbing Greenstone Belt, Western Australia: Structural control on synorogenic- and weathering-related magnetite-, hematite-, and goethite-rich iron ore. *Econ. Geol.* **2010**, *105*, 917–945. [CrossRef]
213. Duuring, P.; Hagemann, S.G.; Novikova, Y.; Cudahy, T.; Laukamp, C. Targeting iron ore in banded iron formations using ASTER data: Weld Range Greenstone Belt, Yilgarn Craton, Western Australia. *Econ. Geol.* **2012**, *107*, 585–597. [CrossRef]
214. Angerer, T.; Hagemann, S.; Danyushevsky, L. High-grade iron ore at Windarling, Yilgarn Craton: A product of syn-orogenic deformation, hypogene hydrothermal alteration and supergene modification in an Archean BIF-basalt lithostratigraphy. *Minim. Depos.* **2012**, *48*, 1–32. [CrossRef]
215. Cassidy, K.F.; Champion, D.C.; Huston, D.L. Crustal evolution constraints on the metallogeny of the Yilgarn Craton. In Proceedings of the Eight Biennial SGA Meeting, Beijing, China, 8–21 August 2005; 2000; pp. 901–904.
216. Bateman, R.; Bierlein, F.P. On Kalgoorlie (Australia), Timmins–Porcupine (Canada), and factors in intense gold mineralisation. *Ore Geol. Rev.* **2007**, *32*, 187–206. [CrossRef]
217. Hronsky, J.A.; Groves, D.; Loucks, R.; Begg, G. A unified model for gold mineralisation in accretionary orogens and implications for regional scale exploration targeting methods. *Minim. Depos.* **2012**, *47*, 339–358. [CrossRef]
218. Cox, S.F. Deformational controls on the dynamics of fluid flow in mesothermal gold systems. In *Fractures, Fluid Flow and Mineralization*; McCaffrey, K., Lonergan, L., Wilkinson, J., Eds.; Geological Society: London, UK, 1999; pp. 123–140.